Gondwana Research 28 (2015) 837–857

Contents lists available at ScienceDirect

Gondwana Research

journal homepage: www.elsevier.com/locate/gr

Geology, geochemistry and geochronology of the Cretaceous Lascano East intrusive complex and magmatic evolution of the Laguna Merín basin, Uruguay

F. Cernuschi [a,b,*], J.H. Dilles [a], A.J.R. Kent [a], G. Schroer [b,1], A.K. Raab [b,2], B. Conti [b,3], R. Muzio [c]

[a] College of Earth, Ocean, and Atmospheric Sciences, Oregon State University, 104 CEOAS Admin Bldg, Corvallis, OR 97331-5506, USA
[b] Was at Orosur Mining Incorporated, Montevideo, 11500, Uruguay
[c] Universidad de la República Oriental del Uruguay, Facultad de Ciencias, UDELAR. Iguá 4225, 11400 Montevideo, Uruguay

ARTICLE INFO

Article history:
Received 22 March 2014
Received in revised form 10 July 2014
Accepted 10 July 2014
Available online 15 August 2014

Handling Editor: T. Kusky

Keywords:
Paraná LIP
Alkaline ring complexes
Cretaceous
Laguna Merín basin
Uruguay

ABSTRACT

The Cretaceous Laguna Merín rift basin in southeastern Uruguay formed during the opening of the southern Atlantic Ocean, and is filled with igneous rocks that we characterize here by field, age, geochemical, and geophysical studies. Initial bimodal magmatic suites (~134 to 128 Ma) include volcanic rocks and intrusions of the sub-alkaline Paraná–Etendeka large igneous province as well as mildly alkaline (transitional) suites. This was followed by younger (~128 to <127 Ma) alkaline gabbro and trachyte intrusions. Ten units of sub-alkaline, transitional, and alkaline rocks can be distinguished by whole rock composition and Nb/Zr ratios, which increase from 0.05 to 0.37 as alkalinity increases. The early sub-alkaline basalts are widespread throughout the Laguna Merín basin, however, later sub-alkaline rhyolites and more alkaline rocks are localized near four ~20 to 30 km diameter ring complexes named Valle Chico, Lascano West, Lascano East and San Luis. Each of the four complexes has a positive gravity anomaly (~80 mGals) and cospatial aeromagnetic anomaly (~1200 nT) with an abrupt margin interpreted as a ring fault. Modeling suggests that the gravity anomalies result from shallowly emplaced and dense gabbro dikes and sills, and additional underlying and more voluminous intrusions extending to more than 5 km depth. The magnetic anomalies correspond to syenites exposed at Valle Chico and sub-alkaline basalts and gabbro dikes at Lascano East. Trace element modeling indicates that the sub-alkaline magmas formed via large degrees of partial melting of shallow mantle sources, whereas the alkaline magmas formed via lower degrees of partial melting of deeper asthenospheric mantle, with progressive deepening of the mantle sources through time. Sr and Nd isotopic compositions of $^{144}Nd/^{143}Nd < 0.5126$ and $^{87}Sr/^{86}Sr > 0.705$ evidence crustal contamination even for the most primitive magmas.

1. Introduction

The opening of the South Atlantic Ocean in the Cretaceous is associated with the eruption of flood basalts and associated rhyolites of the Paraná and Etendeka large igneous provinces in South America and Africa, respectively (Erlank et al., 1984; Bellieni et al., 1986; Hawkesworth et al., 1999). Ring complexes composed of gabbro, alkali gabbro, and felsic intrusion and associated with bimodal basalt–rhyolite volcanic rocks of both sub-alkaline and alkaline compositions are well-exposed and studied in Namibia on the African margin. Ring complexes are also present on the South American margin, but are generally more poorly exposed and studied. Four ring complexes in coastal Uruguay are identified via aeromagnetic surveys, and below we present new geochemical and age data on these igneous rocks. These new data allow us to address the petrogenesis and evolution of the igneous rocks, and more specifically the relationship between the Paraná large igneous province basalts and the sub-alkaline to alkaline ring complex centers within the evolving rifted continental margin.

The bimodal Paraná–Etendeka large igneous province was erupted between 133 and 130 Ma with peak eruption rates between 133 and 132 Ma (Renne et al., 1992; Turner et al., 1994; Stewart et al., 1996; Renne et al., 1997; Deckart et al., 1998; Ernesto et al., 1999; Mincato et al., 2003). This province is dominated by tholeiitic basalt with minor rhyolite. Most workers consider that magmatism is related to the Tristan da Cunha mantle plume and the volcanic rocks at the Rio Grande Rise and the Walvis Ridge (O'Connor and Duncan, 1990). The alternative hypothesis invokes large degrees of melting of subcontinental lithospheric mantle without a mantle plume (Hawkesworth et al., 1988; Peate and Hawkesworth, 1996). In addition to the Paraná volcanics, contemporaneous and younger alkaline ring intrusive complexes are also described in Brazil, Bolivia, Paraguay, Uruguay and Namibia

* Corresponding author at: College of Earth, Ocean, and Atmospheric Sciences, Oregon State University, Oregon, 104 CEOAS Admin Bldg, Corvallis, OR 97331-5506, USA. Tel.: +1 213 309 2990.
E-mail address: cernuscf@geo.oregonstate.edu (F. Cernuschi).
[1] Now at Kinross Gold Corp, Regional Director Exploration BF, Cerro Colorado 5240, Torres del Parque, Las Condes, Santiago—Chile.
[2] Now at Raab Consulting. Carlos Peña Otaegui 9648, Las Condes, Santiago, Chile.
[3] Now at Administración Nacional de Combustibles, Alcohol y Portland—ANCAP, Av. Del Libertador s/n°,Montevideo, Uruguay.

http://dx.doi.org/10.1016/j.gr.2014.07.007
1342-937X/

(e.g., Jacupiranga in Brazil, Velasco province in Bolivia, Valle Chico in Uruguay and the Damaraland province in Namibia; Darbyshire and Fletcher, 1979; Almeida, 1983; Fletcher and Beddoe-Stephens, 1987; Morbidelli et al., 1995; le Roex et al., 1996; Comin-Chiaramonti et al., 1999; Muzio, 2000; Comin-Chiaramonti et al., 2002; Biondi, 2003; Gomes and Comin-Chiaramonti, 2005; Miller, 2008). The complexes along the southeast coast of Uruguay intruded the aborted rifts of the Precambrian basement, that resulted in the formation of the east-northeastly aligned Santa Lucía and Laguna Merín basins. These basins accumulated sequences of Cretaceous volcanic and sedimentary rocks and were grouped under the name of SALAM (Santa Lucía-Aiguá-Laguna Merín, Rosello et al., 1999, Fig. 1).

In comparison to other alkaline provinces, the poorly exposed magmatic rocks of the SALAM have not been comprehensively studied by linking geochemical, geophysical and geochronological data with field observations. The Laguna Merín basin preserves the largest volume of volcanic and intrusive rocks of the SALAM and the availability of drillhole core data and geophysical surveys over the basin offers the opportunity to study its geology and magmatic processes in detail. The Laguna Merín basin presents a large, broad gravity anomaly of >80 mGal and a coincident magnetic anomaly of ~1200 nT (Servicio Geográfico Militar, 1973). The gravity anomaly is approximately 80 km long by 40 km wide, ellipsoidal in shape and elongated in an east to northeast direction (Fig. 2A). High-resolution airborne gravity and magnetic images from Orosur Mining Inc. (OMI), show that this anomaly comprises four well-defined, 20–30 km diameter circular features extending from the town of Mariscala to the Laguna Merín lagoon near the border with Brazil (Ellis and Turner, 2006, Fig. 2B,C). The southwestern anomaly is ~20 km wide and coincident with the syenite outcrops of the Valle Chico intrusive complex (Ferrando and Fernández, 1971). The two central anomalies, named here Lascano West and Lascano East, are each about 20 km in diameter and are coincident with two sub-circular outcrops of rhyolite ignimbrites. The northeastern anomaly, named here San Luis, is the largest at more than 30 km in diameter and is only exposed at its southern edge as granodiorite granophyres and gabbro sills.

Many hypotheses have been proposed to explain both the regional gravity anomaly, and the newly identified gravity and magnetic circular anomalies that constitute it, but they have only been supported by limited surface mapping and one 1000 meter drillhole (DDH502 in Puerto Gómez, DINAMIGE, Gómez Rifas and Masquelin, 1996; Turner et al., 1999). The interpretations range from concealed mafic intrusions similar to Bushveld or Trumpsberg (e.g. Reitmayr, 2001; Veroslavsky et al., 2002), several kilometers of basalt basin filling (Gómez Rifas and Masquelin, 1996) and, for the West and Lascano East anomalies, caldera structures within the Paraná rhyolite sequence (Rosello et al., 1999; Conti, 2008).

The three eastern geophysical anomalies are in areas of limited surface outcrops, but recent drilling at the Lascano East anomaly provides new geologic and geochemical data to study the nature of the anomalies. Below we test the hypothesis that all four of the geophyisical anomalies are produced by intrusive complexes comparable to Valle Chico, the well-exposed western anomaly. We present new data on igneous lithologies that includes surface geologic mapping, drill-hole logging, whole rock major and trace element geochemical analyses, Nd and Sr isotope analyses and isotopic ages, and use these to constrain the age and petrogenetic processes that produced the observed magmatic diversity of the Laguna Merín basin.

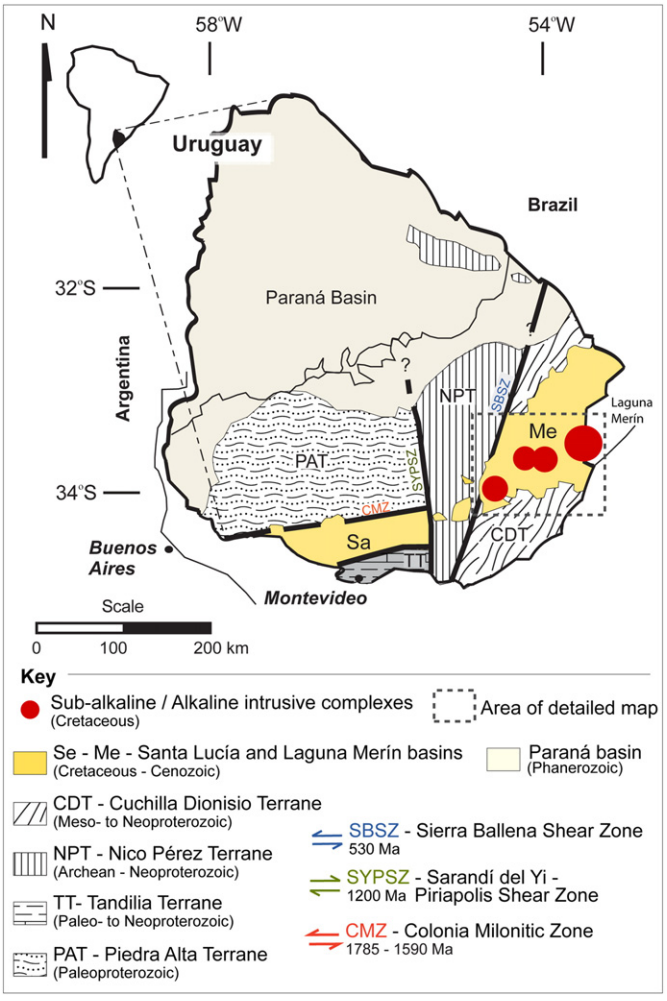

Fig. 1. Schematic geologic map of Uruguay, modified from Bossi et al. (1998) and Bossi et al. (2005). The location of Cretaceous intrusive complexes is from this work.

2. Geologic setting

2.1. Basement rocks

Precambrian rocks crop out over most of southern Uruguay, as well as in two small windows through the Phanerozoic Paraná basin in the north. The basement consists of the Piedra Alta, Tandilia, Nico Pérez and Cuchilla Dionisio terranes, which are bounded by crustal scale shear zones (e.g. Bossi and Gaucher, 2004; Mallman et al., 2004, Fig. 1).

The Chuchilla Dionisio terrane underlies the Laguna Merín basin and is bounded on the west by the Nico Pérez terrane along the Sierra Ballena shear zone (see Bossi et al., 1998; Masquelin, 2006, for a comprehensive review of the Precambrian in Uruguay). The oldest rocks of the Cuchilla Dionisio terrane consist of a Mesoproterozoic granulite to orthogneiss (PGN) core with minor biotite gneisses and migmatites (Preciozzi et al., 1999; Basei et al., 2011, Fig. 3). These rocks are overlain by the Neoproterozoic (~630 to 543 Ma) turbidite sequences of low grade meta-sandstones and -siltstones of the Rocha Formation (Sánchez-Bettucci and Mezzano, 1993; Gaucher et al., 2009). Several granitoids, ranging in age from 850 to 550 Ma (see Oyhantçabal et al., 2009), intrude the older rocks (e.g. Rocha Granite of 762 ± 8 Ma, Hartmann et al., 2002, and Aiguá Granite of 587 ± 16 Ma, Basei et al., 2000). The periphery of the studied area is dominated by the youngest of these intrusions, the coarse-grained feldspar porphyritic Santa Teresa granodiorite (STGD), which has an age of 543 ± 5 Ma (Basei et al., 2013).

2.2. The Laguna Merín basin

The Laguna Merín basin (Fig. 3) preserves the majority of the igneous rocks associated with the Cretaceous rifting in southern Uruguay. Here, we collectively refer to the preserved early Cretaceous (~133 Ma to 127 Ma) volcanic and sedimentary rocks as the Laguna Merín basin sequence, although the basin also includes Cenozoic sedimentary

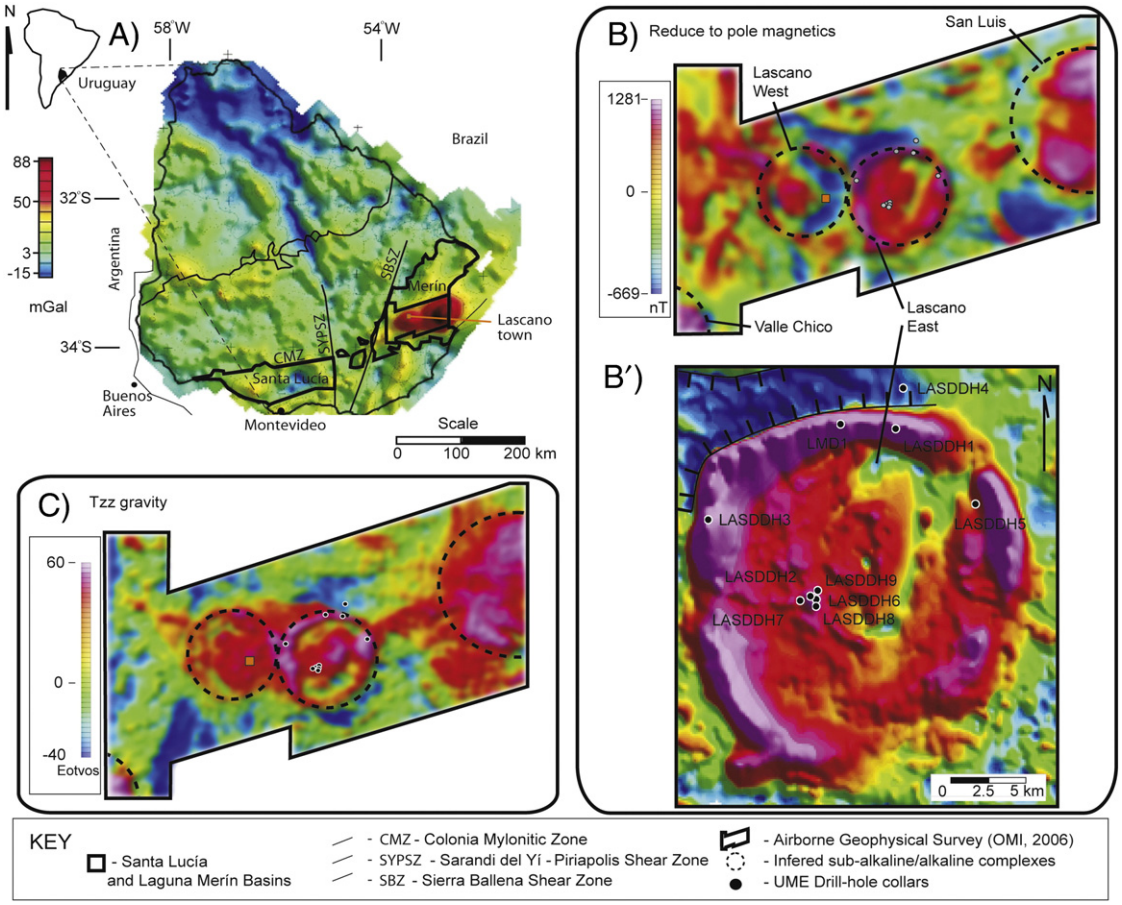

Fig. 2. Geophysical images from Uruguay and the Laguna Merín basin. A) Bouguer anomaly map of Uruguay from regional gravimetry survey (scale 1:1,000,0000, Servicio Geográfico Militar, 1973) adapted from Ellis and Turner (2006) showing location of principal Precambrian structures, Santa Lucía and Laguna Merín basins and location of the geophysical airborne survey shown in B and C. B) Reduce to pole magnetic map, and B′) blown up of B over Lascano East complex. C) Tzz gravity map adapted from Ellis and Turner (2006) and showing the location of interpreted intrusive complexes and location of drillhole collars over Lascano East anomaly. Data from Bellgeospace airborne survey comprising 10,400 km of flight line at a line spacing of 400 m (Orosur Mining Inc.) and using a Geometrics® cesium vapor magnetometer, an Air-FTG® (full-tensor gravity gradiometrer) and a radar altimeter system for terrain corrections. A base station magnetometer was located near Punta del Este.

rocks. Most areas of low relief consist of dark-grey to reddish plagioclase porphyritic and glomeroporphyritic basaltic flows of the Puerto Gómez Formation (Bossi, 1966), later renamed as the Mariscala Formation (Bossi et al., 1998). These basalts infill the rift with documented thicknesses of at least 500 m (Gómez Rifas and Masquelin, 1996).

Overlying the Mariscala basalts in areas of higher topographic relief there are sections up to 200 m thick of quartz-sanidine porphyritic or aphyric rhyolite lava flows, pyroclastic breccias and rheomorphically deformed rhyolitic and rhyodacitic ignimbrites of the Arequita Formation (Bossi, 1966; Morales et al., 2006).

Gabbros and granodiorites intrude the basalts and rhyolites. The San Miguel granodioritic granophyres (Bossi, 1966) range from porphyritic to equigranular and crop out at the east end of the Laguna Merín basin near the border with Brazil and locally at Lascano and are commonly intruded by pyroxene–plagioclase–olivine gabbro sills (Conti, 2008; Muzio et al., 2009).

Prior to this study, the 20 km wide Valle Chico syenite complex was the only known intrusive complex in the Laguna Merín basin (Muzio, 2000; Lustrino et al., 2005). Its outcrop area is coincident with the westernmost circular gravity and magnetic anomaly (Fig. 2B,C).

The Laguna Merín basin lacks the sedimentary diversity observed at the more westerly Santa Lucía basin, and only local conglomerates (<500 m thick) were identified in this work. In the Santa Lucía basin a >2 km sedimentary infill of red-colored polymictic and sandy alluvial conglomerate, organic-rich lacustrine claystone and siltstone that grade upwards into alluvial and aeolian arkosic sandstone is intercalated with the Mariscala basalts and records an arid continental climate during the rifting and magmatism (Bossi, 1966).

The Mariscala and Arequita Formations, in the Laguna Merín basin and elsewhere in the SALAM, were subdivided by Gómez Rifas and Masquelin (1996) and Kirstein et al. (2000) into several lithogeochemical units based on geochemical and petrographic characteristics. Alkaline basaltic lavas cropping out between the Santa Lucía and Laguna Merín basins were assigned to the Marmarajá series by Gómez Rifas and Masquelin (1996). Kirstein et al. (2000) defined two groups of basalts and two groups of rhyolites, including lavas and pyroclastic rocks, for the entire SALAM. These include the sub-alkaline Treinta y Tres basalts and Lavalleja rhyolite series; and the mildly alkaline Santa Lucía basalts and Aiguá rhyolite series. This study expands the lithogeochemical approach of Kirstein et al. (2000) but also includes additional field observations and cross-cutting relations used to define new units and characterize other volcanic and intrusive rocks of the Laguna Merín basin. New names were given to some of the lithogeochemical units to avoid confusion with previously published formal geologic names according to international stratigraphic guidelines (Salvador, 1994).

3. Methods

Reconnaissance geologic mapping of the ring complexes was conducted at a 1:250,000 scale. Detailed core logging and geochemical sampling were conducted on ten 500 to 1000 meter deep vertical cores from holes drilled at Lascano East between 2002 and 2008 by OMI (see the

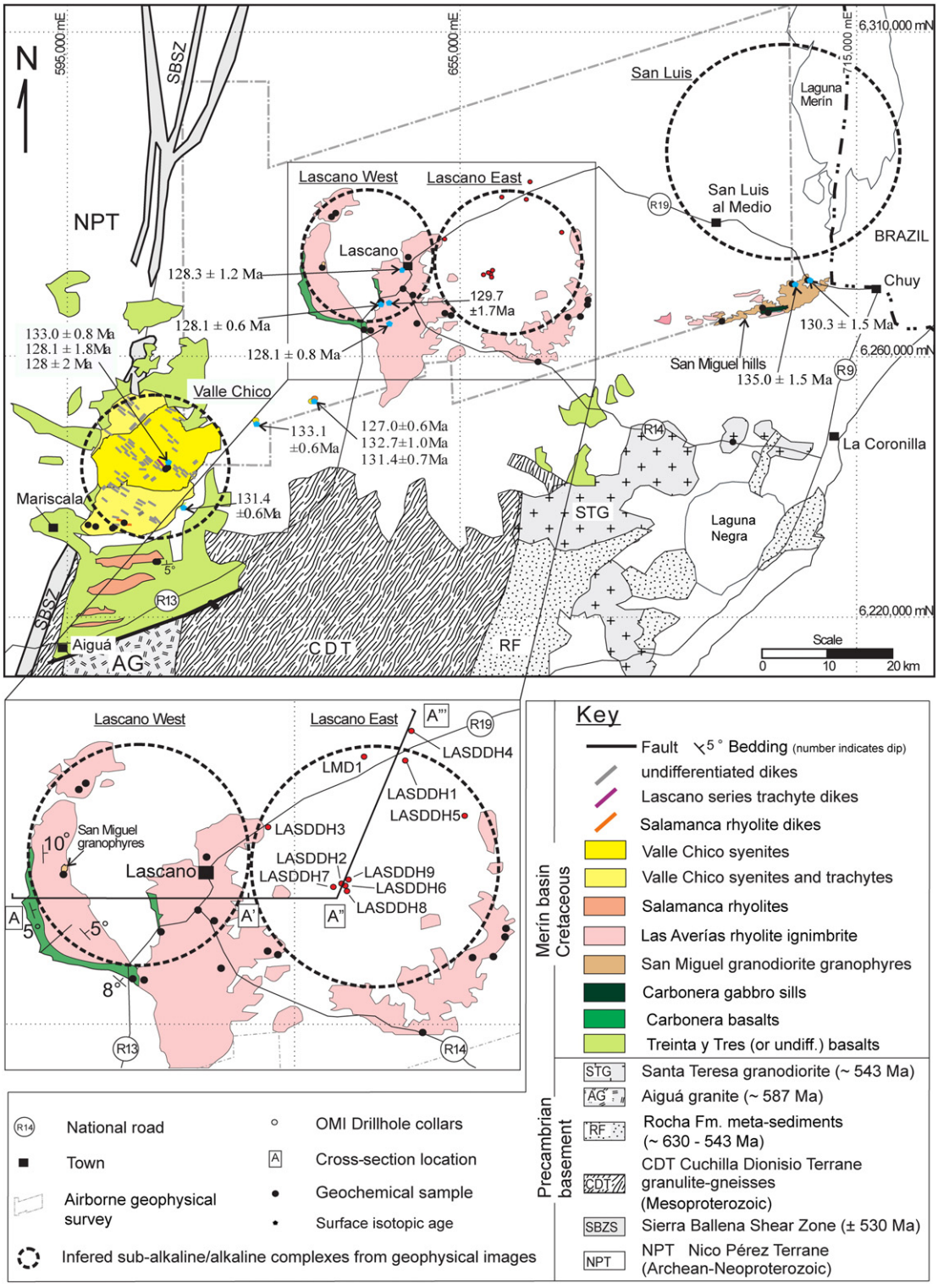

Fig. 3. Geologic map of Laguna Merín basin and its surrounding basement, modified form Bossi and Ferrando (2001), Lustrino et al. (2005), Morales (2006), Conti (2008) and Muzio et al. (2009), showing the location of the interpreted intrusive complexes. Insert shows Lascano West and East and the location of Orosur Mining Inc. drillhole collars. Coordinate system in Gauss-Krugger, Datum Yacaré.

Appendix). Magnetic and gravity images used in this paper are extracted from Ellis and Turner (2006).

Standard transmitted and reflected light microscopy and petrographic techniques were used to describe the mineralogy and textures of the rocks. Magnetic susceptibility was measured throughout the entire core by OMI during drilling using a KT-9 Kappameter portable magnetic susceptibility meter. Specific gravity was measured in representative samples of the magmatic units by measuring dry mass and mass in water with a hydrostatic scale (see Table 1 for data and additional details).

Seven hundred and sixty-five split drill core samples of up to 1 meter long together with 36 surface samples (801 samples) were analyzed at ACME laboratories using inductively coupled plasma optical emission spectrometry (ICP-OES) for major elements and inductively coupled

plasma mass spectrometry (ICP-MS) for trace elements. Lithium metaborate/tetraborate fusion was followed by dissolution using a dilute nitric digestion for ICP-OES and nitric acid digestion for ICP-MS. See Table 2 and the Appendix for additional analytical details and data.

Samples were screened for alkali changes due to hydrothermal alteration using molar ratio diagrams including Na/Al and K/Al (Madeisky and Stanley, 1993), and the remaining 523 fresh samples were selected for lithogeochemical and petrological characterization. Major elements were normalized to 100% volatile-free as presented in Table 2.

The freshest samples were used for age determinations and were inspected in thin section for signs of alteration and analyzed with a CAMECA SX-100 Electron Microprobe at OSU using energy dispersive spectrometry to confirm plagioclase and sanidine compositions. Sanidine and plagioclase separates were prepared at Oregon State University (OSU) from five samples using standard procedures (see Salisbury et al., 2010). Plateau ages from 12 to 22 incremental heating steps of three plagioclase concentrates and one sanidine concentrate were obtained via $^{40}Ar/^{39}Ar$. Analyses were made at OSU Noble Gas Mass Spectometry lab using a Mass Analyser Products model 215–50 rare gas mass spectrometer with all-metal extraction system, after irradiation in the OSU TRIGA experimental reactor (see Koppers and Duncan, 2003). Inverse isochrons ($^{36}Ar/^{39}Ar$ vs. $^{39}Ar/^{40}Ar$) were used to identify excess argon. Plateau ages were calculated as the weighted mean of eight or more consecutive heating steps, representing at least 58% of the released gas. Errors are reported at 2 standard errors of the mean and listed with the MSWD (see Appendix).

Five zircon separates where analyzed to determinate U–Pb ages: two at the Arizona LaserChron Center (University of Arizona) using a laser ablation multicollector ICP-MS (see Gehrels et al., 2006) and three at OSU using a laser ablation quadrupole ICP-MS (see Farmer, 2012; Loewen and Kent, 2012). Zircons were imaged with the cathodoluminescence detector of the CAMECA SX-100 Electron Microprobe at OSU to identify inherited cores and overgrowth rims (see Appendix). Concordant ages within error of one another (n = 8 to 32) are reported as weighted mean ages with a standard error of the mean reported at 2 standard deviation. Analysis in both laboratories used a NewWave 193 nm Excimer laser system with He sweep gas, operating at 4 Hz with a 30 μm fixed spot. General techniques are outlined in Dumitru et al. (2013) for the analyses done at OSU and in Gehrels et al. (2008) for the analyses done at the Laserchron Center. Analyses were standardized using PL-1 zircon at OSU and Sri Lanka zircon at the LaserChron Center, and $^{206}Pb/^{207}Pb$, $^{206}Pb/^{238}U$ and $^{207}Pb/^{235}U$ ratios for each individual analysis were linearly extrapolated to the start of ablation to correct for laser-induced fractionation. Analysis of zircon 91–500 throughout the analysis session (n = 7) at OSU produced a mean $^{206}Pb/^{238}Pb$ ratio of 0.1765 ± 0.0050 (2.1%, 2 se), within <2% of the accepted value for this material.

Nine whole rock samples where analyzed at the University of Cape Town for Sr and Nd isotopic ratios using a NuPlasma high resolution multicollector ICP-MS and standardized to BHVO-2 and NIST 987 (see le Roex et al., 2012 for additional details).

4. Results

4.1. Petrology and geochemistry

The igneous rocks of the Laguna Merín basin can be differentiated based on their petrography (Table 1), whole rock compositions (Tables 1 and 2), and isotopic (Table 3) and relative ages based on cross-cutting relations into three groups according to their alkalinity: sub-alkaline, transitional (mildly alkaline) and alkaline.

Based on whole rock compositions of SiO_2 and alkalis ($NaO + K_2O$, Fig. 4) of the freshest rock samples, the sub-alkaline rocks present a bimodal compositional distribution that includes two types of tholeiitic Paraná type gabbros, basalts, and minor basaltic andesites and a group of dacites, rhyolites and trachy-dacites. The mafic rocks range from ~48 to 54 wt.% SiO_2 and 2 to 4 wt.% $NaO + K_2O$, and the felsic rocks range from ~75 to 77 wt.% SiO_2 and 6 to 10 wt.% $NaO + K_2O$. The transitional igneous rocks present a bimodal compositional trend that partially overlaps with the sub-alkaline rocks in terms of silica and alkalis, however, the samples plot close to the boundary of the sub-alkaline and alkaline fields (Fig. 4). The transitional gabbros and basalts range from ~46 to 52 wt.% SiO_2 and 2 to 5 wt.% $NaO + K_2O$, and the rhyolites and syenites range from ~60 to 79 wt.% SiO_2 and 8 to 11 wt.% $NaO + K_2O$. Whereas the sub-alkaline and transitional groups present bimodal compositions, the alkaline rocks form a continuous compositional range from alkaline gabbro to trachyte (Fig. 4). The alkaline gabbros and basalts range from ~44 to 51 wt.% SiO_2 and 3 to 7 wt.% $NaO + K_2O$. The trachyandesites and trachydacites range from ~55 to 63 wt.% SiO_2 and 8 to 12 wt.% $NaO + K_2O$.

The major element whole rock concentrations of the freshest samples were useful to establish the grouping of the different magmatic units based on their alkalinity (Fig. 4), however, alkalis are sensitive to remobilization by hydrothermal alteration, which affects some of the rocks in the study area. The whole rock concentrations of trace elements together with petrographic and cross-cutting relations were used to define ten lithogeochemical units. In particular, immobile and incompatible Nb and Zr define a series of distinctive magmatic Nb/Zr ratios (Figs. 5, 6). Nb and Zr are found in high concentrations in the studied samples (Nb 2–160 ppm, Zr 30–750 ppm) enabling precise measurements of their concentrations. The Nb/Zr ratios vary by up to a factor of 3 between successive lithogeochemical groups, and are used here as the primary basis of distinction.

The sub-alkaline rocks (Fig. 5), include the plagioclase–clinopyroxene–olivine–magnetite Treinta y Tres basalts (Nb/Zr = 0.05) and Carbonera basalts-gabbros (Nb/Zr = 0.09); the plagioclase–quartz–clinopyroxene–amphibole San Miguel granodiorite granophyres (Nb/Zr = 0.10) and the quartz–sanidine–plagioclase Las Averías rhyolite ignimbrites (Nb/Zr = 0.07). The Treinta y Tres basalts unit as used here was defined by Kirstein et al. (2000) (Fig. 6), and is named for outcrops east to the Treinta y Tres town. The newly defined Carbonera basalts–gabbros, are petrographically similar to the Treinta y Tres basalts, but are characterized by higher Nb/Zr compositional ratios (Fig. 6). Compared to the Treinta y Tres basalts, the Carbonera basalts are less commonly exposed but they are ubiquitous in the subsurface of Lascano East. The Carbonera unit also includes gabbro dikes and sills, but no gabbros of Treinta y Tres composition have been reported. We introduce the new name the Las Averías rhyolite ignimbrites for rocks corresponding to the Lavalleja series defined by Kirstein et al. (2000) (Fig. 6). The proposed name change is justified because the name Lavalleja has been previously used for other lithostratigraphic units, and the characteristic rhyolites are not common at the Lavalleja locality but are common at the Las Averías hills in the Laguna Merín basin. The San Miguel granodiorite granophyres were defined by Bossi (1966), who did not report data on their chemical composition.

The transitional rocks (Fig. 5), include the plagioclase–clinopyroxene–olivine–magnetite Coronilla basalts–gabbros (Nb/Zr = 0.14); the quartz–sanidine–plagioclase Salamanca rhyolites (Nb/Zr = 0.15); the India Muerta rhyolites (Nb/Zr = 0.11); and the K-feldspar–plagioclase–amphibole–pyroxene–magnetite Valle Chico syenites (Nb/Zr = 0.13). The Coronilla basalts–gabbros as defined here partially correspond to the Santa Lucía basalts defined by Kirstein et al. (2000) (Fig. 6), however, the Santa Lucía unit included samples of basalts from outside of the Laguna Merín basin. Furthermore, the name has been previously used to define the Cretaceous Santa Lucía basin in southwestern Uruguay (Fig. 1), where there are also basalts of similar age. To avoid confusion we refer to the Laguna Merín basin basalts with Nb/Zr = 0.14 as Coronilla basalts. This unit also includes gabbro sills that were not previously described for Santa Lucía. The Salamanca rhyolites as defined here correspond to the Aiguá rhyolite series defined by Kirstein et al. (2000) (Fig. 6), however, we drop the name Aiguá because it has been previously used for the Precambrian granitoids that crop out at the Aiguá town. The type locality of these rhyolites is defined for the Salamanca caves (Grutas

Table 1
Petrographic descriptions and physico-chemical properties of igneous and sedimentary rocks of the Merín Basin.

Formation	Lithogeochemical unit	Rock type	Thickness (m)	Magmatic lineage	Emplacement type	Mineralogy	Texture	SiO_2 wt% min max	T. Alk. wt% min max	Nb/Zr avg. min max	CIPW norm	Density Sample	Density (g/cc)	Mag. sucept. (x 10^{-3}SI)
Quebracho	N.A.	Conglomerates, sandstones.	< 400	clasts: sub-alkaline	N.A.	N.A.	60% , 3mm-30cm clasts (60% basalt, 40% rhyolite). Clast-supported. 20%, 0.3 mm angular sandy matrix (qtz>lithic>px>plg). 20% ceolitic matrix. Fining upwards in metric cycles.	N.A.	N.A.	clasts 0.06 0.16	N.A.	N.D.	N.D.	< 15
Arequita	Arrayán olivine basalts	basalts	flows:1–10 < 200	alkaline	lavas	40% cpx, 20% ol, 30% plg, 5% mgt, 4% hm, ap <1%	10 %, 1-5 mm ol phen, sparse 1 mm plg phen. 0.05-0.3 mm matrix. Variolitic txt. Sparse 1-20 mm vugs.	47.77 50.82	3.42 4.87	0.36 0.23 0.47	undersaturated ol - hyp. Normative	N.D.	N.D.	< 15
	Lascano alkaline series	trachyandesites to trachydacites	< 15	alkaline	dikes, sills	65 - 77 % plg, 25% k-fd, 1 - 9% qtz, < 1% mgt, 1% ap.	20%, 0.5 - 4 mm K-fd/plg phen. 0.01 - 0.1 ground mass with 0.1-0.5 k-fd and plg microlites. Often pilotaxitic banding.	54.77 63.70	8.61 11.89	0.23 0.12 0.28	undersaturated nepheline normative	71951	2.54	< 15
		trachybasalts /gabbros	< 10			75% plg, 14% px, 2%bt, 5% mgt, 1% ap.	15%, 0.5 - 6 mm plg/px ppy. 0.1 - 0.5 ground mass	44.07 51.46	3.18 6.94			80002	2.99	80 - 110
	Valle Chico syenites	syenites, qtz-syenites, granites, trachytes	?	transitional to locally peralkaline	Lacolith, ring-complex?	70% K-fd, 10 plg, 2 to 10% qtz, 1 to 5% px, 0 to 5% amph, 1%bt, 1% mgt.	0.5-20 mm equigranular	59.85 - 61.15	8.38 8.88	0.13 0.12 0.15	oversaturated quartz normative	71954	2.41	25 - 200
	Salamanca rhyolites	rhyolites	flows ± 1	transitional	dikes, flows.	10% qtz, 25% sa, 10% plg, <1% ap, 54% aph. matrix.	40 % 1-10 mm sa±qtz ppy in aphanitic matrix. Thin flows are usually aphanitic.	61.0 79.0	8.40 12.2	0.15 0.20 0.10		71959	2.54	N.D.
	India Muerta rhyolites		2 – 100		dikes, sills, domes?	15% qtz, 20% sa, 10% plg, <1% ap, 54% aph. matrix.	15%, 0.2-3 mm qtz ppy and/or 30% 1-20 mm sa ppy in aphanitic matrix.	67.32 73.54	7.78 10.57	0.11 0.09 0.17		N.D.	N.D.	< 10
	Las Averías rhyolites		< 200 < 100 < 20 < 80	sub-alkaline	ignimbrites, rheoignimbrites, dikes, pyroclastic breccias	10% qtz, 15% sa, 15% plg, <1% ap, <1zir, 53% aph. matrix.	5% 0.2-3 mm qtz and 5% 1-3 mm plg phen. Shards, lithoclasts and elongated pumice clasts. up to 20% 1-3 mm plg phen. Aphanitic to vitrophyric. Sparse plg-san phen. Angular clasts < 2 m	67.21 76.94	6.34 9.11	0.07 0.05 0.13		71959 N.D.	2.54 N.D.	< 10
	San Miguel granodiorite granophyres	granodiorites	> 700	sub-alkaline	sills, domes?	70% plag, 20% qtz, 5% cpx, 5% amph, <1% mgt, <1% ap.	10% 2-5 mm plg phen in 0.3 to 1 mm matrix with plg-qtz granophyric intergrows. 0.1 to 1 mm eq. Granophyric plg-qtz intergrows.	65.53 - 70.30	7.06 9.61	0.10 0.06 0.10		71956	2.46	< 8
Puerto Gómez / Mariscala	Coronilla basalts and gabbros	basalts	flows 5–15 >600	transitional	lavas	58% plg, 30% cpx, 5% ol, 6% mgt, 1% ap.	20%, plg ppy (10%, 5-10 mm xenocrysts, euhedral plg and 10%, 3-5 mm plag). 0.1-1 mm Intersitial plg, ol, cpx, mgt, ap. Oph texture.	46.29 52.38	2.41 5.02	0.14 0.12 0.17	undersaturated olivine - hypersthene normative to oversaturated quartz normative	basalt 73082	2.67	60 - 130
		gabbros	<200		dikes, sills	58% plg, 26% cpx, 5% ol, 10% mgt, 1% ap.	up to 3 mm subhedral plg and interstitial subhedral px and ol. Common mgt/hm euhedral crystals forming in tabular intersitial zones.					gabbro 73088	2.99	100 - 200
	Carbonera basalts and gabbros	basalts	flows 3–10 >800	sub-alkaline	lavas	60% plg, 25% cpx, 10% ol, 1% ap, 5%	Aph or 1-10 mm plg phen. Rare px 1-5 mm phenos. 0.1-1 mm int. to s-oph matrix	48.23 54.42	2.10 4.27	0.09 0.06 0.12		N.D.	N.D.	40 - 60
		gabbros	< 350		dikes, sills	60% plg, 25% cpx±opx, 10% ol, 1% ap, 5% mgt	up to 3 mm cummular equigranular					gabbro 71968	2.93	
	Treinta y Tres basalts *	basalts	flows 3–10 >600	sub-alkaline	lavas	45% plg, 45 % mesostasis, 5% cpx, 5% mgt.	Aph or 1-15mm plg ppy/gppy in 0.1-0.2 mm matrix with vitreous mesostasis. 20 mm voids.	49.24 53.81	2.89 4.05	0.05 0.04 0.06		N.D.	N.D.	100 - 200

Abbreviations: ap (apatite), bi (biotite), cpx (clinopyroxene), mgt (magnetite), ol (olivine), plg (plagioclase), san (sanidine), k-fd (potassic feldspar), qtz (quartz), zir (zircon), ppy (porphyritic), eq. (equigranular), aph (aphanitic), gppy (glomeroporphyritic), phen (phenocrystals), oph (ophitic), s-oph (sub-ophitic), hyp. (hypersthene), T. Alk. ($Na_2O + K_2O$), N.D. (No Data), N.A. (Not applicable), Mag. Sucept. (Magnetic suceptibility). * Modified from Kirstein et al. (2000). Notes: Specific gravity was calculated as S.G. = Mass(air) / [Mass(air) − Mass(water)], and density was calculated as ρ = S.G. × ρ(water), where ρ(water) = 1.0 g/cc. CIPW normative compositions were estimated using Kurt Hollocher's excel program (NORMS). KT-9 Kappameter portable magnetic susceptibility meter detection limit of 1×10^{-3} S.I.

de Salamanca). The India Muerta rhyolites are newly defined here to include the transitional rhyolitic dikes and sills that are only found in the subsurface of Lascano East. The name Valle Chico was previously defined for the syenites as the Valle Chico Formation by Ferrando and Fernández (1971).

The alkaline rocks (Fig. 5) include the plagioclase–clinopyroxene–biotite–magnetite trachybasalts and plagioclase–K-feldspar–quartz trachyandesites to trachydacites of the newly defined Lascano alkaline series (Nb/Zr = 0.23); and the clinopyroxene–olivine–plagioclase–magnetite of the newly defined Arrayán olivine basalts (0.18 < Nb/Zr < 0.47). No lava flows of Lascano series affinity have been identified in the Laguna Merín basin, however, Gómez Rifas and Masquelin (1996) described isolated basalt lava flows and dikes of similar composition in the Marmarajá hills between the Santa Lucía and Laguna Merín basins (Fig. 1).

The Quebracho Formation is newly defined here to include conglomerates and sandstones with angular to rounded mafic and felsic volcanic clasts up to 0.5 m diameter.

Besides Nb and Zr, the concentrations and ratios of other relatively immobile high field strength elements such as Ti, P, Sc, Ta, Hf, Th, Y and rare earths are characteristic of each unit. The sub-alkaline Treinta y Tres basalts and Carbonera basalts–gabbros have overlapping patterns on mantle normalized diagrams plots (Fig. 8A,B), whereas the transitional Coronilla basalts–gabbros are enriched in alkalis, alkaline earths (Cs, Rb, Ba, Sr) and high field strength elements such as Ta, Nb, La and Hf. In comparison to the Coronilla basalts, these elements are more enriched in the gabbros of the Lascano alkaline series and even more enriched in the Arrayán olivine basalts (Fig. 8C,D).

The Arrayán olivine basalt is the most distinctive geochemical unit. Whereas all the other mafic units have rare earth patterns relatively similar to an Enriched Mid-Ocean Ridge Basalt composition (E-MORB), the Arrayán basalt patterns are similar to an Ocean Island Basalt (OIB) as shown by relatively strong depletions in heavy rare earths compared to light rare earths (Fig. 7D). In comparison with present day OIB magmatism at Tristan da Cunha and Gough island, the Arrayán olivine basalts are generally less enriched in trace elements (Fig. 8B). Another difference is that the Arrayán basalts are the only mafic rocks that have a small positive Eu anomaly whereas all the other mafic units have a negative anomaly (Fig. 7C). The sub-alkaline Las Averías rhyolite ignimbrites and the San Miguel granodiorite granophyres have overlapping patterns in spider plots whereas the transitional Salamanca and India Muerta rhyolites, the alkaline Valle Chico syenites and the Lascano series trachytes are relatively enriched in heavy rare earths and high field strength elements such as Ta, Nb, La, Nd, Hf and Zr (Fig. 7E,F,G).

Isotopic compositions for the three different geochemical groups are also distinct from each other. All groups have $^{144}Nd/^{143}Nd < 0.5126$ and $^{87}Sr/^{86}Sr > 0.705$ (Table 2), which indicates that even the basaltic igneous rocks have been contaminated by neodymium and strontium derived from continental crust. The sub-alkaline and transitional mafic rocks present the lowest $^{144}Nd/^{143}Nd$ and highest $^{87}Sr/^{86}Sr$ ratios evidencing more crustal contamination, whereas the alkaline mafic rocks are the least contaminated rocks. The OIB-like Arrayán olivine basalts show the highest $^{144}Nd/^{143}Nd$ and lowest $^{87}Sr/^{86}Sr$.

4.2. Geochronology

The new U–Pb zircon and $^{40}Ar/^{39}Ar$ ages, as well as previous published ages, for all the dated igneous rocks range between 134 and 127 Ma and are summarized in Table 3. Errors are reported with 2 standard deviations. The $^{40}Ar/^{39}Ar$ plateau ages and inverse isochrons together with age spectra, concordia and probability plots for U–Pb zircon ages are available in the appendix.

The $^{40}Ar/^{39}Ar$ ages of plagioclase and sanidine (n = 4) have weighted mean plateaus produced by more than 58% of the ^{39}Ar gas released and corresponding MSWDs that range between 0.04 and 0.57. Three of the samples present three to four initial heating steps that yield younger ages than the plateau. These steps are attributed to Ar-loss in the rims of the crystal grains, they represent less than 20% of the ^{39}Ar gas release and were discarded for the age calculation. These samples are: 80002 (Lascano alkaline series gabbro, 127.8 ± 0.9 Ma in plagioclase), 80006 (India Muerta rhyolite, 129.1 ± 0.5 Ma in sanidine) and 79992 (Las Averías rhyolite, 129.0 ± 0.18 Ma in plagioclase). Sample 71907 (Treinta y Tres basalt, plagioclase) is the only sample that shows excess Ar for the first 4 heating steps, representing 41% of the ^{39}Ar released. Nonetheless, for sample 71907 59% of the Ar released yield a robust plateau age of 126.94 ± 0.89 Ma, which agrees with the isochron age of 126.98 ± 1.36 Ma.

U–Pb in zircon ages for each sample were calculated using only the individual zircon spot analyses that produced a gaussian distribution and lying within two standard deviations of the mean. This mean age is interpreted as the age of cooling and crystallization of the rock. All the samples present at least one and up to eleven individual zircon spot analyses that yield younger or older ages, outliers of the gaussian distribution of ages. The younger ages are considered to be produced by Pb-loss, and the older ages to be produced by inherited or antecrystic grains. Inherited grains were confirmed by several spot analyses of zircon cores with ages as old as 165 Ma (Appendix). We use the weighted mean of concordant individual zircon ages and consider it robust for all the samples, based on MSWDs ranging between 0.94 and 1.4. The best ages are 131.10 ± 0.73 Ma for sample LASRV (India Muerta rhyolite) calculated from 26 individual analyses, and 134.25 ± 0.56 Ma for sample LASGR (San Miguel granodiorite granophyre) calculated from 32 individual analyses. The other three ages were calculated from fewer individual analyses, but are considered robust and yield ages consistent with other ages. Sample 79999 (San Miguel granodiorite granophyre) yields an age of 133.97 ± 0.75 Ma calculated from 14 individual analyses, sample SM049 (San Miguel granodiorite granophyre) yields an age of 130.3 ± 1.5 Ma calculated from 8 individual analysis, and sample SM004 (San Miguel granodiorite granophyre) yields an age of 135.0 ± 1.3 Ma calculated from 8 individual analysis

4.3. Density and magnetic susceptibility

The three types of gabbros (Carbonera, Coronilla and Lascano alkaline series), have the highest density, up to 2.99 g/cc (see Table 1 for details). The gabbros are considerably denser than the compositionally similar basalts. For example, the Coronilla gabbros have a density of 2.99 g/cm^3, and are about ~0.32 g/cm^3 denser than the 2.67 g/cm^3 Coronilla basalts. All the felsic rocks have a density between 2.41 and 2.54 g/cm^3 and are therefore at least 0.45 g/cm^3 less dense than the gabbros.

All the mafic units, except the Arrayán olivine basalts, have a high magnetic susceptibility up to 200×10^{-3} SI, however, the sub-alkaline Carbonera basalts and gabbros are slightly less magnetic than other units. The felsic rocks have very low susceptibility, commonly under the detection limit of the instrument (1×10^{-3} SI). A notable exception is the Valle Chico syenite that has a high magnetic susceptibility similar to the most magnetic mafic unit (200×10^{-3} SI, Ellis and Turner, 2006).

5. Discussion

Whereas the sub-alkaline Treinta y Tres and Carbonera basalts are widespread through the Laguna Merín basin, the rest of the igneous rocks are spatially restricted and likely genetically related to the four ring complexes (Figs. 3 and 8). Whereas the Valle Chico complex is mainly composed of syenite exposures, the other three complexes are concealed under volcanic rocks, younger sediments and soil. From southwest to northeast the concealed complexes are named here Lascano West, Lascano East and San Luis.

Table 2
Selected representative chemical analysis.

Lithogeochemical unit	Sample	HoleID	From (m) or latitude coord. (m)	To (m) or longitud coord. (m)	SiO_2 wt.%	Al_2O_3 wt.%	Fe_2O_3 w%	MgO w%	CaO w%	Na_2O w%	K_2O w%	TiO_2 w%	P_2O_5 w%	MnO w%	Cr_2O_3 w%	LOI wt%	Ba ppm	Ce ppm	Co ppm	Cs ppm	Cu ppm	Dy ppm	Er ppm	Eu ppm	Ga ppm	Gd ppm	Hf ppm	Ho ppm
Treinta y Tres basalts	71907	LMD1	−433.7	−434.7	50.26	17.54	10.94	4.78	10.51	2.71	1.22	1.63	0.22	0.18	0.02	4.5	305	35.4	39.5	0.6	61.3	5.3	3.1	1.6	20.9	5.1	4.0	1.1
	71932	LASDDH1	−624.35	−625.35	51.29	16.01	11.92	4.93	10.50	2.42	1.14	1.41	0.16	0.18	0.03	1.8	263	32.9	42.7	0.2	119.0	5.0	3.0	1.3	17.5	4.9	3.3	1.0
	71905	LMD1	−196.4	−197.4	55.68	15.70	10.08	3.65	8.65	2.64	1.97	1.28	0.16	0.15	0.03	2.0	420	53.4	33.7	0.4	45.8	5.1	3.1	1.5	19.1	5.6	5.8	1.1
Carbonera	71902	LASDDH3	−286.7	−287.7	48.76	15.47	11.19	8.70	12.37	2.07	0.26	0.85	0.05	0.19	0.09	3.1	72	7.1	53.0	0.4	117.4	2.6	1.6	0.7	14.9	2.1	0.9	0.6
gabbros-basalts	73060	LASDDH5	−120	−121	50.57	17.02	9.86	7.62	10.62	2.51	0.70	0.83	0.06	0.14	0.07	3.7	167	22.7	42.5	0.8	127.1	3.4	2.2	0.9	14.5	3.2	2.3	0.7
	73067	LASDDH5	−400.3	−401.2	53.14	15.73	10.27	6.44	9.24	2.55	1.32	0.98	0.14	0.15	0.04	2.7	268	32.3	38.7	0.8	124.1	4.8	3.3	1.2	16.7	4.3	3.9	1.1
San Miguel granodiorite	73066	LASDDH5	−340.5	−341.25	64.60	13.63	7.76	1.91	3.50	3.06	4.24	0.93	0.23	0.10	0.03	1.2	704	85.5	13.4	2.9	60.8	9.2	6.1	1.7	16.9	8.7	9.6	2.0
granophyres	73063	LASDDH5	−200	−200.95	67.63	12.78	6.04	1.04	3.51	2.88	5.05	0.76	0.18	0.09	0.03	3.0	704	92.7	8.5	3.9	28.6	9.2	6.2	1.7	14.4	8.8	10.3	2.0
	79999	LASDDH5	−200	−200.95	67.63	12.78	6.04	1.04	3.51	2.88	5.05	0.76	0.18	0.09	0.03	3.0	704	92.7	8.5	3.9	28.6	9.2	6.2	1.7	14.4	8.8	10.3	2.0
	LASGR	LASDDH8	−791	−792	67.91	14.14	4.89	0.93	1.94	3.24	5.89	0.79	0.15	0.07	0.05	2.2	775	105.2	8.9	4.4	26.3	8.1	5.2	1.1	18.3	8.1	16.0	1.7
Las Averías rhyolite	79992	LASDDH4	−637.3	−638.3	70.28	12.66	5.98	1.16	1.49	2.14	5.27	0.67	0.20	0.10	0.03	2.7	922	112.0	6.8	2.9	7.9	8.9	4.9	1.9	16.2	9.3	10.0	1.8
ignimbrite	73107	LASDDH4	−637.3	−638.3	70.28	12.66	5.98	1.16	1.49	2.14	5.27	0.67	0.20	0.10	0.03	2.7	922	112.0	6.8	2.9	7.9	8.9	4.9	1.9	16.2	9.3	10.0	1.8
	71960	surface	6266807	652522	71.52	12.79	5.76	0.30	1.49	2.00	5.16	0.64	0.17	0.08	0.08	1.7	1480	132.2	7.1	3.1	10.7	10.7	6.3	2.4	17.3	11.5	10.6	2.2
India Muerta rhyolites	73414	LASDDH6	−618.8	−619.8	69.06	14.56	4.27	0.26	1.51	4.60	5.13	0.41	0.06	0.09	0.03	1.3	953	134.4	2.4	0.7	12.1	17.0	10.7	2.2	21.2	14.1	19.9	3.5
	71928	LASDDH1	−406.6	−407.5	74.12	12.00	3.98	0.09	1.40	2.39	5.62	0.22	0.03	0.06	0.09	0.0	1366	170.7	2.3	1.7	6.9	12.6	7.0	2.2	18.6	13.4	11.1	2.4
	80006	LASDDH1	−406.6	−407.5	74.12	12.00	3.98	0.09	1.40	2.39	5.62	0.22	0.03	0.06	0.09	0.0	1366	170.7	2.3	1.7	6.9	12.6	7.0	2.2	18.6	13.4	11.1	2.4
	LASVR	LASDDH3	−310	−311	73.55	12.40	4.04	0.09	1.62	2.78	5.08	0.28	0.05	0.06	0.04	0.7	1420	124.5	1.4	2.9	3.2	9.7	5.5	2.2	17.9	10.3	13.0	1.9
Valle Chico syenites	71953	Surface	6235033	604924	66.30	14.79	6.70	0.81	1.07	3.48	5.40	1.00	0.30	0.12	0.03	1.7	1341	122.6	8.1	1.4	9.7	9.1	5.5	2.2	22.0	9.2	11.2	1.8
	71994	Surface	6243231	611116	63.88	14.23	8.33	1.08	2.13	3.55	4.81	1.36	0.46	0.15	0.00	2.2	1272	115.4	10.6	2.0	12.8	6.7	4.2	2.2	21.4	7.3	11.2	1.3
Salamanca rhyolites	71977	surface	6229151	609779	76.28	11.98	3.01	0.22	0.21	2.79	5.11	0.27	0.09	0.05	0.00	2.3	126	287.0	1.2	4.8	5.2	15.6	9.2	0.5	26.0	16.5	18.4	3.2
	71975	surface	6206293	549289	77.78	11.28	2.53	0.05	0.36	2.51	5.27	0.17	0.03	0.02	0.00	1.5	252	163.6	0.6	1.0	6.4	9.1	5.3	0.6	22.4	7.9	12.3	1.9
Coronilla gabbros	73086	LASDDH2	−498.3	−499.3	47.22	14.47	15.97	4.91	10.51	2.65	0.79	2.92	0.31	0.22	0.02	3.3	237	36.5	45.0	0.1	98.1	7.3	4.4	1.9	19.9	6.7	4.1	1.5
and basalts	73131	LASDDH6	−217.23	−218.23	50.35	16.87	12.53	3.82	9.78	3.21	0.95	1.96	0.31	0.16	0.06	2.2	257	35.8	34.3	0.2	147.2	6.7	4.3	1.8	20.1	6.4	4.7	1.4
	73128	LASDDH6	−214.23	−215.23	49.92	18.63	11.38	3.40	10.42	3.19	0.82	1.79	0.28	0.12	0.04	2.1	242	31.5	32.7	0.1	89.5	6.1	3.8	1.7	20.4	5.8	4.4	1.3
Lascano alkaline series	80002	LASDDH7	−219.8	−220.8	47.36	17.04	12.39	4.45	9.97	3.91	1.46	2.52	0.67	0.20	0.03	1.5	481	56.3	33.4	0.3	52.3	6.6	3.5	2.4	20.6	7.1	4.4	1.3
(trachybasalts)	71940	LASDDH7	−219.8	−220.8	47.36	17.04	12.39	4.45	9.97	3.91	1.46	2.52	0.67	0.20	0.03	1.5	481	56.3	33.4	0.3	52.3	6.6	3.5	2.4	20.6	7.1	4.4	1.3
	71535	LASDDH8	−214.05	−215	48.83	15.37	13.08	3.91	7.66	4.63	2.19	2.89	1.15	0.27	0.01	1.7	642	76.9	26.2	7.8	24.8	9.6	5.2	3.3	20.7	10.0	6.0	1.9
Lascano alkaline series	71611	LASDDH8	−738.55	−739.55	55.26	17.01	10.91	1.29	4.49	5.70	3.37	1.28	0.41	0.26	0.01	4.0	764	97.7	7.6	0.2	14.6	13.2	8.3	3.6	28.9	12.2	11.8	2.7
(trachyandesites)	71617	LASDDH8	−744.55	−745.55	55.57	16.35	11.09	1.51	4.65	5.64	3.02	1.40	0.47	0.30	0.00	2.9	714	92.4	8.7	0.5	19.2	12.5	7.6	3.6	24.4	12.0	11.6	2.6
	71619	LASDDH8	−746.55	−747.55	56.05	16.17	11.04	1.48	4.48	5.40	3.23	1.39	0.47	0.27	0.01	2.6	766	92.0	8.3	0.4	18.3	12.3	7.7	3.6	25.1	11.7	11.6	2.6
Lascano alkaline series	73442	LASDDH6	−677.35	−678.25	60.15	15.99	8.24	0.51	2.56	5.16	6.28	0.74	0.14	0.22	0.00	2.0	635	69.5	1.3	0.3	5.6	8.1	4.8	2.3	24.2	7.9	7.7	1.6
(trachydacites)	73083	LASDDH2	−149.1	−150.1	61.42	15.11	8.33	0.38	2.64	5.55	5.56	0.69	0.13	0.19	0.01	2.2	284	81.3	1.4	0.8	7.8	9.1	5.2	1.7	18.3	8.4	8.2	1.8
	71577	LASDDH8	−549.65	−550.65	63.31	15.89	6.95	0.35	2.07	5.51	5.28	0.43	0.05	0.17	0.00	2.0	462	117.4	0.5	0.4	5.1	14.8	9.2	2.2	28.3	13.3	16.3	3.1
Arrayán olivine basalts	73103	LASDDH4	−458.6	−459.6	47.78	15.20	11.27	9.67	9.84	2.89	1.00	1.50	0.62	0.16	0.07	5.8	583	61.6	45.9	9.4	55.9	3.3	1.5	1.6	16.3	4.1	3.5	0.6
	73102	LASDDH4	−420.5	−421.5	49.49	14.83	11.48	6.78	12.35	2.74	0.69	1.23	0.23	0.16	0.04	8.1	249	24.6	42.4	2.6	120.8	3.2	1.6	1.2	15.9	3.3	2.2	0.6
	73101	LASDDH4	−205.5	−206.5	49.68	15.76	10.06	8.19	8.84	2.98	1.89	1.82	0.59	0.13	0.06	5.7	598	55.3	37.4	3.3	48.1	3.4	1.8	1.6	16.6	4.3	4.3	0.7
Pre-Є gneiss (PGN)	71979	Surface	6222863	617933	70.96	14.48	3.64	0.82	2.08	3.16	4.12	0.51	0.17	0.06	0.00	2.1	1596	98.1	9.3	19.4	5.0	3.6	2.1	1.5	17.0	4.1	6.9	0.7
Pre-Є granodiorite (STGD)	71986	Surface	6247336	695338	75.11	13.53	2.15	0.28	0.46	3.15	4.90	0.25	0.13	0.05	0.00	1.1	248	88.2	1.9	32.7	2.0	5.8	3.6	0.6	22.3	5.4	4.7	1.2
Volcanic clasts in	73054	LASDDH4	−398.2	−402.4	53.74	15.11	11.75	5.04	8.40	3.46	0.70	1.40	0.19	0.17	0.03	6.1	312	34.2	36.8	0.9	63.3	4.3	2.5	1.3	18.8	4.6	3.3	0.9
Quebracho	73055	LASDDH4	−404.45	−406.45	54.44	14.19	12.78	4.99	7.30	2.78	1.16	1.89	0.22	0.23	0.01	5.8	379	61.3	40.0	0.9	35.6	6.6	3.8	1.7	20.9	6.9	5.7	1.3
Conglomerate	73056	LASDDH4	−218.4	−233	57.96	13.24	10.95	5.44	6.60	3.34	0.77	1.35	0.15	0.19	0.01	7.6	459	52.7	39.0	1.1	47.2	5.5	3.2	1.4	21.2	5.9	4.9	1.2

Notes: Coordinates in Gauss-Krugger, Datum Yacaré. Location of Drillholes in the Appendix. Major elements were measured at ACME labs using a Spectro Ciros® Vision ADS500 ICP-OES and reported as oxides with a 0.002 to 0.04 wt.% detection limit. Trace elements were measured with an Elan® 9000 ICP-MS and detection limits vary between 0.01 and 0.5 ppm for most of the elements (see Appendix). n.d. = no data. BDL = below detection limit. Pre-Є = Precambrian.

Table 2 (*continued*)

Lithogeochemical unit	La ppm	Lu ppm	Mo ppm	Nb ppm	Nd ppm	Ni ppm	Pb ppm	Pr ppm	Rb ppm	Sc ppm	Sm ppm	Sn ppm	Sr ppm	Ta ppm	Tb ppm	Th ppm	Tm ppm	U ppm	V ppm	W ppm	Y ppm	Yb ppm	Zn ppm	Zr ppm	$^{143}Nd/^{144}Nd$	$^{87}Sr/^{86}Sr$	$^{87}Sr/^{86}Sr$ (*130 Ma)	$^{143}Nd/^{144}Nd$ (*130 Ma)
Treinta y Tres basalts	15.7	0.4	0.1	7.3	20.1	48.0	1.6	4.8	34.2	33	4.9	1.0	263.3	0.4	0.9	2.0	0.5	0.4	272	BDL	29.4	2.9	58	148.0	0.512475	0.708977	0.708299	0.512346
	14.4	0.4	BDL	6.4	18.2	43.0	1.8	4.3	34.8	39	4.2	1.0	187.9	0.4	0.8	3.2	0.5	0.5	282	BDL	26.8	2.9	38	143.8	n.d.	n.d.	n.d.	n.d.
	24.7	0.4	BDL	9.0	28.3	28.0	2.6	6.7	59.7	31	5.7	BDL	204.0	0.5	0.9	5.8	0.5	0.8	205	BDL	30.5	3.0	57	178.9	n.d.	n.d.	n.d.	n.d.
Carbonera	3.0	0.3	0.1	3.4	5.1	109.0	0.6	1.0	6.0	46	1.6	BDL	180.1	0.2	0.4	0.5	0.3	BDL	298	BDL	15.8	1.6	37	39.3	n.d.	n.d.	n.d.	n.d.
gabbros-basalts	10.2	0.3	1.5	8.3	12.1	162.0	3.3	2.9	18.4	36	2.7	1.0	211.7	0.4	0.6	3.2	0.4	0.4	222	0.6	21.6	2.2	47	71.0	0.512325	0.711326	0.710962	0.512204
	15.1	0.5	0.3	11.3	18.4	93.0	2.8	4.3	39.3	35	4.2	2.0	191.0	0.7	0.8	3.5	0.5	0.7	218	0.5	29.8	3.0	46	132.5	n.d.	n.d.	n.d.	n.d.
San Miguel granodiorite	41.1	0.9	1.5	25.1	40.4	21.0	5.8	10.7	135.6	20	8.6	3.0	120.1	1.7	1.5	13.2	0.9	2.0	89	1.4	57.7	5.6	80	320.2	n.d.	n.d.	n.d.	n.d.
granophyres	45.3	0.9	0.9	28.3	44.9	BDL	10.2	11.3	168.9	13	9.1	3.0	89.0	1.7	1.6	15.9	1.0	2.2	48	1.9	58.7	5.7	60	353.7	0.512215	0.723291	0.719945	0.512107
	45.3	0.9	0.9	28.3	44.9	BDL	10.2	11.3	168.9	13	9.1	3.0	89.0	1.7	1.6	15.9	1.0	2.2	48	1.9	58.7	5.7	60	353.7	n.d.	n.d.	n.d.	n.d.
	50.2	0.7	1.7	41.9	45.3	BDL	11.3	12.1	253.1	9	8.3	5.0	91.1	2.8	1.4	27.7	0.8	4.0	50	1.5	48.7	5.0	55	573.8	n.d.	n.d.	n.d.	n.d.
Las Averías rhyolite	55.8	0.8	0.7	22.5	50.3	BDL	7.6	13.8	169.0	13	10.1	3.0	87.8	2.6	1.6	17.2	0.8	2.7	29	1.6	48.5	4.8	69	357.6	n.d.	n.d.	n.d.	n.d.
ignimbrite	55.8	0.8	0.7	22.5	50.3	BDL	7.6	13.8	169.0	13	10.1	3.0	87.8	2.6	1.6	17.2	0.8	2.7	29	1.6	48.5	4.8	69	357.6	0.512070	0.735566	0.732218	0.511963
	67.9	0.8	0.8	22.1	70.2	BDL	5.1	17.5	181.7	12	12.7	3.0	118.7	1.4	1.9	18.6	0.9	2.5	32	1.6	65.1	5.9	71	356.2	n.d.	n.d.	n.d.	n.d.
India Muerta rhyolites	64.3	1.8	3.0	78.8	68.9	BDL	7.3	16.7	141.0	9	13.3	6.0	81.9	4.3	2.7	15.3	1.8	2.9	16	0.9	103.2	12.3	92	724.3	n.d.	n.d.	n.d.	n.d.
	80.1	1.0	0.2	33.5	80.8	BDL	3.6	21.2	206.9	6	15.4	4.0	111.5	1.9	2.2	24.0	1.1	2.7	BDL	0.6	65.8	6.6	24	378.5	0.512109	0.725871	0.721772	0.512007
	80.1	1.0	0.2	33.5	80.8	BDL	3.6	21.2	206.9	6	15.4	4.0	111.5	1.9	2.2	24.0	1.1	2.7	BDL	0.6	65.8	6.6	24	378.5	n.d.	n.d.	n.d.	n.d.
	63.5	0.9	0.6	26.0	66.2	BDL	3.0	17.4	187.1	7	12.0	3.0	122.6	1.9	1.7	15.6	0.9	2.1	BDL	0.7	54.6	5.7	29	482.9	n.d.	n.d.	n.d.	n.d.
Valle Chico syenites	57.6	0.8	1.8	55.5	54.2	BDL	14.1	14.1	163.4	13	10.0	3.0	222.7	3.5	1.6	12.2	0.9	2.5	33	1.0	55.0	5.3	73	445.8	n.d.	n.d.	n.d.	n.d.
	58.2	0.6	3.1	76.8	47.7	20.0	5.2	12.8	133.1	14	8.3	4.0	294.6	4.2	1.2	7.8	0.7	1.4	71	0.8	38.9	4.1	58	409.3	n.d.	n.d.	n.d.	n.d.
Salamanca rhyolites	228.9	1.3	0.8	94.0	189.4	20.0	23.6	54.7	212.4	1	27.4	6.0	24.2	5.7	2.8	21.9	1.4	3.6	46	0.6	89.4	8.9	80	644.2	n.d.	n.d.	n.d.	n.d.
	51.3	0.7	2.0	35.4	41.8	20.0	7.1	12.2	155.5	1	8.4	4.0	29.1	2.0	1.5	15.8	0.8	2.2	10	0.5	54.5	5.2	61	393.7	n.d.	n.d.	n.d.	n.d.
Coronilla gabbros	16.3	0.6	0.7	23.8	23.5	25.0	1.2	5.2	18.2	50	5.8	1.0	263.3	1.3	1.2	2.7	0.7	0.5	631	BDL	42.1	4.2	74	152.7	n.d.	n.d.	n.d.	n.d.
and basalts	16.5	0.6	0.5	25.3	22.2	22.0	0.6	4.8	23.0	38	5.6	1.0	289.4	1.5	1.2	2.5	0.7	0.6	349	1.5	40.0	4.1	65	174.4	0.512595	0.706432	0.705977	0.512460
	15.3	0.6	0.4	22.8	18.5	62.0	0.6	4.3	19.5	34	4.8	2.0	319.9	1.4	1.1	2.3	0.6	0.5	329	61.4	35.4	3.6	57	154.4	n.d.	n.d.	n.d.	n.d.
Lascano alkaline series	28.1	0.5	1.9	49.5	31.6	BDL	2.5	7.3	25.8	23	6.8	1.0	555.1	2.9	1.2	3.4	0.6	0.9	260	0.6	35.8	3.2	75	174.6	n.d.	n.d.	n.d.	n.d.
(trachybasalts)	28.1	0.5	1.9	49.5	31.6	BDL	2.5	7.3	25.8	23	6.8	1.0	555.1	2.9	1.2	3.4	0.6	0.9	260	0.6	35.8	3.2	75	174.6	0.512697	0.704740	0.704229	0.512582
	36.4	0.7	2.3	65.7	43.3	BDL	1.9	9.9	47.2	21	9.8	2.0	445.6	3.8	1.7	3.9	0.8	1.0	168	0.7	50.8	4.6	91	242.3	n.d.	n.d.	n.d.	n.d.
Lascano alkaline series	49.9	1.2	2.8	115.8	52.3	BDL	5.7	12.6	82.7	12	11.9	4.0	139.9	6.5	2.3	8.0	1.3	2.0	BDL	1.6	76.6	7.9	132	487.9	n.d.	n.d.	n.d.	n.d.
(trachyandesites)	47.2	1.1	3.2	106.6	50.6	BDL	4.9	12.1	89.9	13	11.5	3.0	227.0	6.0	2.2	7.4	1.2	2.1	BDL	1.9	73.3	7.5	109	453.5	n.d.	n.d.	n.d.	n.d.
	47.3	1.1	2.8	109.0	49.3	BDL	4.8	11.9	96.9	14	11.2	3.0	175.6	5.9	2.2	6.1	1.2	1.9	BDL	1.7	68.6	7.1	109	462.7	n.d.	n.d.	n.d.	n.d.
Lascano alkaline series	34.4	0.8	3.2	71.3	34.0	BDL	5.7	8.7	144.7	9	7.6	3.0	140.3	4.3	1.4	6.7	0.8	1.6	BDL	0.6	41.3	4.8	79	308.8	n.d.	n.d.	n.d.	n.d.
(trachydacites)	40.4	0.8	2.8	78.2	38.5	BDL	6.6	10.4	114.9	7	8.1	2.0	63.1	4.5	1.5	7.5	0.8	1.7	16	1.2	49.7	5.2	60	340.0	0.512633	0.740745	0.738469	0.512521
	61.5	1.4	1.3	148.0	56.1	BDL	9.0	14.4	154.6	2	12.7	5.0	72.4	8.7	2.5	10.5	1.5	2.8	BDL	1.0	83.4	9.4	123	636.2	n.d.	n.d.	n.d.	n.d.
Arrayán olivine basalts	36.1	0.2	2.0	75.6	25.3	188.0	2.7	6.9	16.3	26	4.6	BDL	708.9	4.0	0.6	4.8	0.2	1.4	186	0.7	16.2	1.4	49	161.0	0.512636	0.704614	0.704292	0.512539
	12.5	0.2	0.4	17.9	13.0	87.0	2.8	3.2	27.3	32	3.3	BDL	432.4	1.0	0.6	1.5	0.2	0.5	205	0.7	16.3	1.5	53	77.0	n.d.	n.d.	n.d.	n.d.
	31.0	0.3	1.3	55.7	24.9	161.0	2.6	6.5	31.1	24	5.1	BDL	587.9	4.1	0.7	4.7	0.3	1.3	168	0.8	18.5	1.6	56	171.5	n.d.	n.d.	n.d.	n.d.
Pre-Є gneiss (PGN)	36.4	0.3	0.2	10.4	31.5	20.0	7.1	8.4	177.6	7	5.2	7.0	380.8	0.4	0.6	6.1	0.3	1.3	46	1.8	17.8	1.8	45	269.6	n.d.	n.d.	n.d.	n.d.
Pre-Є granodiorite (STGD)	39.3	0.7	0.7	35.8	35.5	20.0	6.2	9.8	444.9	4	7.0	23.0	57.2	6.5	1.0	28.3	0.6	6.9	12	7.8	36.1	4.5	28	160.6	n.d.	n.d.	n.d.	n.d.
Volcanic clasts in	20.1	0.3	0.3	18.8	20.7	84.0	3.1	4.8	21.8	31	4.2	1.0	366.0	0.9	0.8	2.6	0.4	1.0	233	1.0	30.6	2.4	48	114.3	n.d.	n.d.	n.d.	n.d.
Quebracho	31.9	0.6	0.1	15.7	34.3	37.0	7.7	8.3	35.7	35	7.1	2.0	274.5	0.9	1.3	8.2	0.6	1.8	298	0.6	44.7	3.6	41	199.3	n.d.	n.d.	n.d.	n.d.
Conglomerate	26.0	0.4	0.2	10.3	29.8	29.0	7.1	7.2	27.8	33	6.2	1.0	353.7	0.5	1.0	6.4	0.5	1.4	257	0.4	37.7	3.1	55	170.0	n.d.	n.d.	n.d.	n.d.

Table 3
Isotopic ages for the Merín Basin.

Formation	Lithogechemical unit	Location (+) drillhole and depth or surface coordinates	Sample number	Method	Mineral	Plateau age/ weighted mean (*)	MSWD	Author
	Lascano alkaline series gabbro	LASDDH7 219 m	80002	$^{40}Ar/^{39}Ar$	plg	127.8 ± 0.9	0.57	This paper
	Valle Chico syenites	611045 mE 6244062mN	93-L-59		n.d.	133.0 ± 0.8	1.0	Stewart et al. (1996)
		n.d.	Mar-55	U/Pb	zirc	128.1 ± 1.8	n.d.	Lustrino et al. (2005)
		n.d.	VC-93			128 ± 2	n.d.	Muzio et al. (1999)
Arequita	India Muerta rhyolites	LASDDH1 407 m	80006	$^{40}Ar/^{39}Ar$	san	129.1 ± 0.5	0.31	This paper
		LASDDH3-329 m	LASRV	U–Pb	zirc	131.10 ± 0.73	0.73	This paper (LaserChron)
	Salamanca rhyolites	632827 mE 6253353mN	93 L28	$^{40}Ar/^{39}Ar$	san	127.0 ± 0.6	1.00	Stewart et al. (1996)
	Las Averías rhyolite ignimbrites	LASDDH4 637 m	79992		plg	129.0 ± 0.6	0.18	This paper
		643981 mE 6268555mN	93 L107		san	128.1 ± 0.6	1.7	Kirstein et al. (2001b)
		642680 mE 6268353mN	93 L105			129.7 ± 1.7	0.7	
		646009 mE 6273850mN	93 L112			128.3 ± 1.2	0.3	
		644024 mE 6265226mN	93 L118			128.1 ± 0.8	2.3	
	San Miguel granodiorite granophyres	LASDDH5 200 m	79999	U–Pb	zirc	133.97 ± 0.75	1.08	This paper (OSU)
		707225 mE 6271843mN	SM049			130.3 ± 1.5	0.94	
		704158 mE 6271391mN	SM004			135.0 ± 1.5	1.30	
		LASDDH8 791 m	LASGR			134.25 ± 0.56	1.08	This paper (LaserChron)
Puerto Gómez / Mariscala	High Nb basalts	632827 mE 6253353mN	93 L53	$^{40}Ar/^{39}Ar$	plg	131.4 ± 0.7	1.5	Stewart et al. (1996)
	[Coronilla / Carbonera ?]	632827 mE 6253353mN	93 L47			132.7 ± 1.0	1.0	Stewart et al. (1996)
	Treinta y Tres basalts	LMD1 434 m	71907			126.9 ± 0.9	0.04	This paper
		624150 mE 6249923mN	93 L93			133.1 ± 0.6	1.60	Stewart et al. (1996)
		613479 mE 6237084mN	93 L42			131.4 ± 0.6	2.0	Kirstein et al. (2001b)

Abbreviations: plg (plagioclase), san (sanidine), zirc (zircon), N.D. (no data), MSWD (Mean Standard Weighted Deviation). Notes: (*) Isotopic ages reported with 2stdev. (+) Location in Gauss-Krugger, Datum Yacaré. Location of drillhole collars in Appendix.

5.1. Geology, geochemistry and isotopic ages

5.1.1. Sub-alkaline rocks

This group generally presents the oldest isotopic ages in the Merín basin. The sub-alkaline basalts of Paraná affinity are the only basalts exposed in the Laguna Merín basin and include the Treinta y Tres basalts (Nb/Zr = 0.051) and the Carbonera basalts (Nb/Zr = 0.090). Both units lie at the same stratigraphic position and are usually aphanitic or present fine-grained plagioclase phenocrysts. They occur as thin, 3 to 10 m thick, lava flows in low relief areas and are overlain by rhyolites near Valle Chico and Lascano East and West. In the subsurface at Lascano East the Treinta y Tres and Carbonera lavas are volumetrically dominant in the periphery of the complex and have composite thicknesses up to 600 m for Treinta y Tres and up to 350 m for Carbonera. Here, hyaloclastically fractured basalt Treinta y Tres lavas (LASDDH4) provides the only evidence for underwater volcanism in the basin.

Whereas the Treinta y Tres basalt type has only been observed as lavas, the Carbonera compositional type also characterizes fine- to medium-grained equigranular gabbro sill-like bodies that intrude the San Miguel granodiorite granophyres. Other Carbonera exposures include some on the northeastern edge of the basin in the San Miguel hills, and in drillhole core from Lascano East where the gabbro sills have thicknesses that range from 1 to 200 m. Both Carbonera gabbros and San Miguel granodiorites are found as xenoliths in the other unit, indicating broadly synchronous emplacement. The identification of the xenoliths as Carbonera gabbros is supported by the similar major and trace element analyses (Fig. 5 and Appendix). The $^{40}Ar/^{39}Ar$ ages of the Treinta y Tres basalts and Carbonera basalt and gabbro and the U–Pb in zircon ages of the San Miguel granodiorite range from 133.97 ± 0.75 to 130.3 ± 1.5. From these units, only one sample of a Treinta y Tres basalt yields a younger age of 126.9 ± 0.9 and its significance is discussed below.

The sub-alkaline Las Averías rhyolites have Nb/Zr values of ~0.065 and comprise a diverse unit. Whereas quartz and/or feldspar porphyritic ignimbrites and rheomorphically deformed ignimbrites containing fiammé, glass shards and lithic clasts dominate at Lascano West exposures; ignimbrites, pyroclastic breccias, vitrophyres and banded feldspar porphyritic rhyolites (flows or volcaniclastic sedimentary rocks) dominate at Lascano East. The Las Averías rhyolites overlie the Carbonera basalt. The rhyolites have a stratigraphic thickness up to 200 m where they are exposed as a topographic ring of outcrops that define the margins of the Lascano East and West ring structures, which furthermore correspond to the circular geophysical anomalies. At Lascano West, the contact of the Las Averías rheo-ignimbrites with the underlying Carbonera basalt lavas, as well as the compaction foliation of rhyolites dip at 2° to 10° towards the center of the ring complex and potentially record deformation related to caldera collapse (Rosello

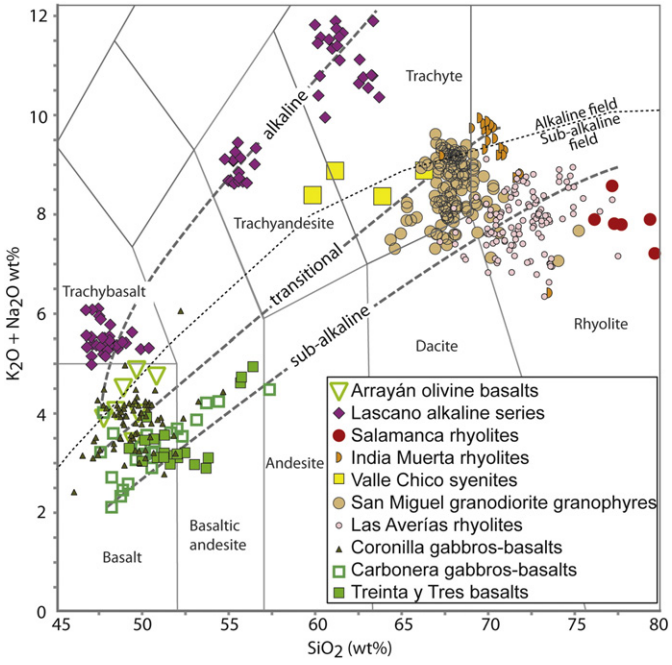

Fig. 4. Total alkalis ($K_2O + Na_2O$) versus silica (SiO_2) (Le Maitre et al., 1989) showing the alkaline/sub-alkaline boundary (Irvine and Baragar, 1971). Only the freshest samples (screened using a Na/Al versus K/Al molar plot) were used to construct this diagram. Three apparent trends are show by the dashed lines: two bimodal trends (one sub-alkaline and one transitional or mildly alkaline) and one continuous alkaline trend.

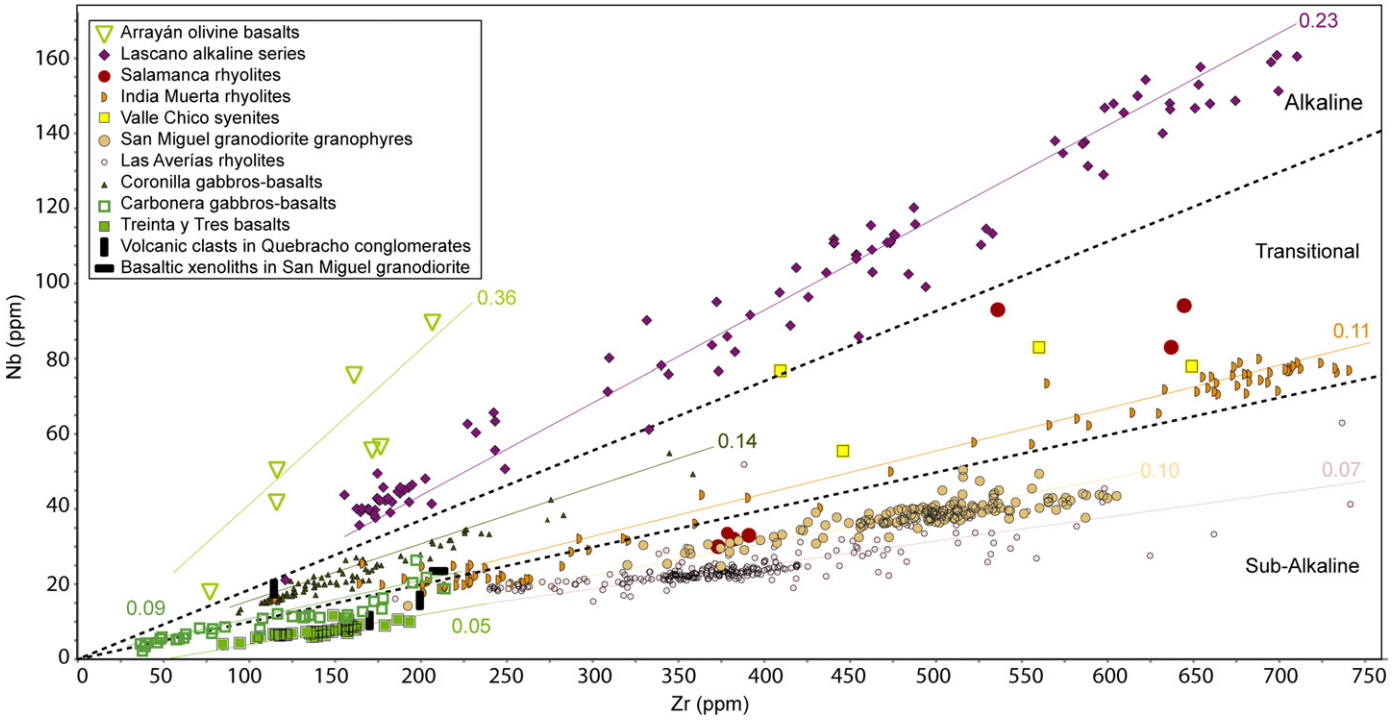

Fig. 5. Zr versus Nb plot of fresh and unaltered rock samples displays linear compositional trends that distinguish several different lithogeochemical units within the igneous rocks of the Laguna Merín basin. The average Nb/Zr ratios and ratio lines are shown for each lithogeochemical group.

et al., 1999; Conti, 2008). The $^{40}Ar/^{39}Ar$ ages of these rhyolites range from 129.7 ± 1.7 to 128.1 ± 0.6 Ma, and are therefore mostly younger than the isotopic ages of the Carbonera basalts and gabbros and related granodiorites (Table 3). In drill core at Lascano East, the Las Averías rhyolites are up to 200 m in thickness and were observed in other stratigraphic positions that include intercalated with Treinta y Tres basalts (LMD1, LASDDH2), on top of Treinta y Tres but underneath Carbonera basalts (LASDDH3), and intercalated with Coronilla basalts (e.g. LASDDH6), which indicates an overlapping age with the basalts.

5.1.2. Transitional rocks

Based on cross-cutting relationships and isotopic ages, the transitional rocks generally overlap or post-date the sub-alkaline rocks but pre-date the alkaline rocks. These units also have Nb/Zr ratios and trace element concentrations intermediate between the sub-alkaline and alkaline groups (Figs. 5, 6).

The Coronilla basaltic lavas are only observed at the subsurface in the center of Lascano East where they are volumetrically dominant (up to 600 m thick, e.g. LASDDH2). The basalts have diagnostic coarse-grained euhedral plagioclase crystals, which in some cases have corroded edges. Equigranular gabbro sills 2 to 20 m thick and with similar compositions cross-cut the basalts in the drill core (e.g. LASDDH2). $^{40}Ar/^{39}Ar$ ages of high Nb basalts that outcrop between Valle Chico and Lascano West (Fig. 3, Stewart et al., 1996) and might correspond to the Coronilla unit, range between 132.7 ± 1.0 and 131.4 ± 0.7 Ma, and overlap in age with the sub-alkaline basalts. However, the Coronilla basalts are also observed intercalated with Las Averías rhyolite ignimbrites in the subsurface of Lascano East, which suggests an age younger than 131 Ma.

The Salamanca rhyolites have Nb/Zr of 0.15 and a $^{40}Ar/^{39}Ar$ age of ~127.0 ± 0.6 Ma. Lavas of similar composition, in the vicinity of Minas, Lavalleja, ~ 60 km West of the Laguna Merín basin have a reported age of 131.9 ± 0.9 Ma (Kirstein et al., 2000). Since these outcrops are not part of the Laguna Merín basin, and the genetic relationship of these lavas with the Salamanca rhyolites is unknown, this age is not considered here. The Salamanca rhyolites range from feldspar and quartz porphyritic to aphanitic and crop out in the elevated topography around the Salamanca caves and other localities surrounding the central syenites of the Valle Chico complex. Most outcrops consist of 1- to 3-m-thick lava flow units, whereas some others contain broken quartz and feldspar crystals that suggest a pyroclastic origin. Nonetheless, no shards or fiammé were identified in these rocks. The less explosive character of the Salamanca rhyolites in comparison with the Las Averías rhyolites has been discussed by Kirstein et al. (2001a). The contact of the Salamanca rhyolites with the underlying Treinta y Tres and Carbonera basalts as well as the contacts between Salamanca flows dip between 3° and 5° to the northwest, towards the center of the Valle Chico complex. Narrow dikes (0.5- to 3-m wide) of similar chemical affinity intrude the Valle Chico syenites. They strike east–west and northwest–southeast and dip 65° to 90° to the north or northeast (Lustrino et al., 2005).

No Salamanca rhyolites were observed at Lascano East, however, dikes and sills of the newly defined India Muerta rhyolites (Nb/Zr = 0.111) are compositionally similar to Salamanca. The India Muerta rhyolites contains euhedral quartz and sanidine phenocrysts and forms 20 to 100 m thick dikes and sills that cross-cut Las Averías rhyolite ignimbrites (LASDDH4), Carbonera gabbros and San Miguel granophyres (LASDDH3), Treinta y Tres basalts (LASDDH7) and Coronilla basalts (LASDDH6). The $^{40}Ar/^{39}Ar$ and U–Pb zircon ages range between 131.10 ± 0.73 and 129.1 ± 0.5 and are older than the isotopic ages of the Salamanca rhyolites.

The Valle Chico syenites (Nb/Zr = 0.130) are exposed only in the ~20 km diameter center of the Valle Chico geophysical anomaly. Here, we include the syenites in the transitional group; however, Lustrino et al. (2005) reported local peralkaline compositions. Two U–Pb ages for the Valle Chico syenites (128.1 ± 1.8 Ma, 128 ± 2 Ma) are younger than the $^{40}Ar/^{39}Ar$ age 133 ± 2 Ma reported previously (Stewart et al., 1996). No raw data, spectra or isochrons are available for this sample and it is not possible to judge the quality of the age, however, based on the stratigraphic and contact observations, we consider the U–Pb ages as the best estimate of Valle Chico syenites.

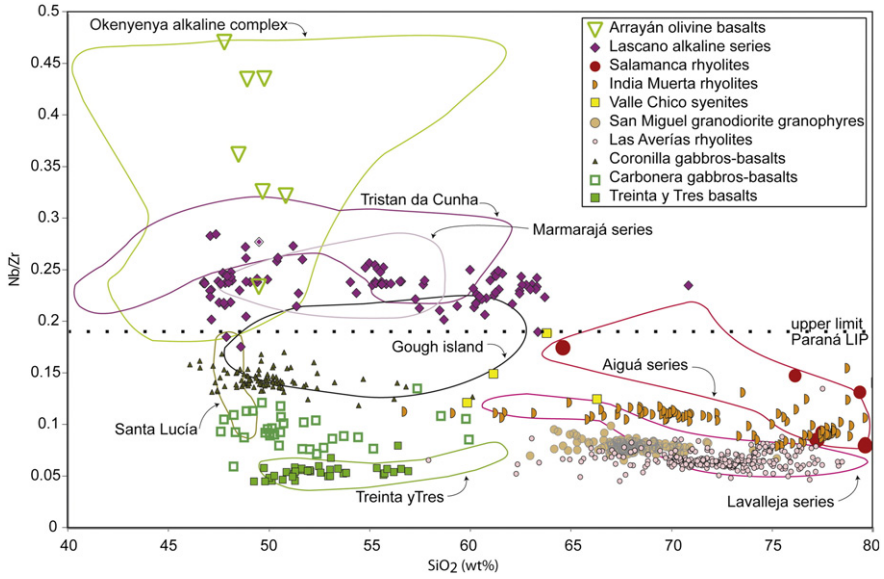

Fig. 6. Nb/Zr versus SiO_2 plot of fresh whole rock samples and comparison with compositional fields Treinta y Tres and Santa Lucía basalts, and Lavalleja and Aiguá rhyolites from Kirstein et al. (2000), Marmarajá series from Gómez Rifas and Masquelin (1996), Tristan da Cunha basalts from le Roex et al. (1990) and gabbro–basalts from Okenyenya complex (Namibia) from le Roex et al. (1996). The upper Nb/Zr limit for the Paraná lavas was calculated using data from GEOROC.

5.1.3. Alkaline rocks

Based on cross-cutting relations these newly recognized alkaline intrusions are the youngest magmas in the basin, and the $^{40}Ar/^{39}Ar$ age of one gabbro from the Lascano alkaline series is 127.8 ± 0.9 Ma. This group also has a restricted Nb/Zr ratio from mafic to felsic rocks that averages Nb/Zr = 0.23.

The Lascano alkaline series intrusions are only observed in drill holes at the center of Lascano East. They cut most of the sub-alkaline and transitional rocks intruding the Coronilla basalts (LASDDH2), the Las Averías rhyolites (LASDDH6) and the San Miguel granodiorite granophyres (LASDDH8). The trachyte dikes and sills range between 10 cm and 15 m wide, whereas the gabbro dikes and sills reach widths of up to 45 m. Similar trachyte dikes have been identified in outcrop at the center of Valle Chico, where they cut the syenites.

The newly identified Arrayán olivine basalts (no isotope ages), have the highest Nb/Zr ratios of the Cretaceous magmas of Uruguay (0.18 < Nb/Zr < 0.47, Fig. 5). These basalts present distinctive 1 to 3 mm olivine phenocrysts partly altered to iddingsite. They were only identified at the subsurface of Lascano East, as 1 to 5 m thick flows, immediately northeast of the Lascano East ring structure. Here, a total of 120 m of basalt flows are intercalated with Quebracho conglomerates and overlie sub-alkaline basalts and rhyolite ignimbrites (LASDDH4).

The Quebracho Formation is newly defined here to include conglomerates and sandstones with angular to rounded mafic and felsic volcanic clasts of up to 0.5 m diameter. This unit does not crop out but reaches 400 m thickness at the periphery of Lascano East. Up to 20 m thick lenses of conglomerate, possibly age correlative but more likely older, have been observed intercalated with the upper lavas of the Coronilla basalts in the central zone of Lascano East (LASDDH7).

Three samples of basalt and rhyolite clasts from the Quebracho conglomerates (LASDDH4), have Nb/Zr ratios between the sub-alkaline and transitional rock ratios, suggesting provenance from units of that composition (Fig. 5). These conglomerates are similar to the Cañada Solís Formation from the Santa Lucía basin (De Santa Ana and Ucha, 1994). However, the Cañada Solís conglomerates lie in a lower stratigraphic position intercalated with Mariscala basalts.

5.2. Age of igneous rocks

The isotopic ages for the dated igneous rocks range between 134 and 127 Ma, with some of the ages overlapping at two standard deviation confidence interval. Nonetheless, when the ages are plotted according to the geographical distribution of the samples and cross-cutting relationships are also taken into account, three age groups become evident (Fig. 9). The magmatism generally evolved from an early phase dominated by sub-alkaline basalts throughout the Laguna Merín basin, to sub-alkaline felsic volcanic rocks and intrusions, and finally by transitional and alkaline magmas localized near the individual ring complexes. Sub-alkaline to transitional basalts and gabbro-granodiorite dikes and sills (Carbonera, Coronilla and San Miguel) dominate between 134 and 130 Ma and are found throughout the basin. Sub-alkaline rhyolite ignimbrites then erupted from 131.5 Ma to 127 Ma (Las Averías) and dominate the areas of Lascano West and East. Lastly, the transitional to alkaline dikes, sills and plugs at Valle Chico and Lascano East range between ~128 Ma to 127 Ma or possibly younger (Valle Chico syenites, Salamanca rhyolites, Lascano alkaline series and India Muerta rhyolites). The Arrayán olivine basalts were not dated, but their age is inferred to be younger than ~127 Ma based on cross-cutting relationships.

A few observations deserve further discussion. The ages of the Treinta y Tres, Carbonera and Coronilla basalts are consistent with most of the field observations that the Las Averías rhyolites stratigraphically overly the basalts. Nonetheless, the exception is one age of ~127 Ma for a Treinta y Tres basalt from Lascano East, which is younger than the age of the Las Averías rhyolites. This age is consistent with field observations of small volumes of the Treinta y Tres, Carbonera and Coronilla basalts stratigraphically overlying the Las Averías rhyolites. We conclude that the sub-alkaline to transitional basaltic magmatism dominated between 134 and 131 Ma but small volumes of this composition erupted as late as 127 Ma. Therefore, basalts with similar chemical affinity were probably erupted at different ages in different parts of the basin. Furthermore, the observed cross-cutting relations evidenced that the alkaline rocks post date the sub-alkaline ones. However the 127 Ma age of one of the sub-alkaline Treinta y Tres basalts overlaps with the isotopic ages of the alkaline rocks suggesting that both types of magmatism were active at the same time at least in some areas of the basin. Similarly, the mildly alkaline Valle Chico syenites and the Salamanca and India Muerta rhyolites, partially overlap in age with the sub-alkaline Las Averías rhyolite ignimbrites.

Based on the isotopic ages, the Lascano alkaline series rocks are younger than the India Muerta rhyolites, however, no cross-cutting observation confirm this hypothesis. At Valle Chico, the syenites intrude the Salamanca rhyolitic lavas, but the isotopic ages of the two units

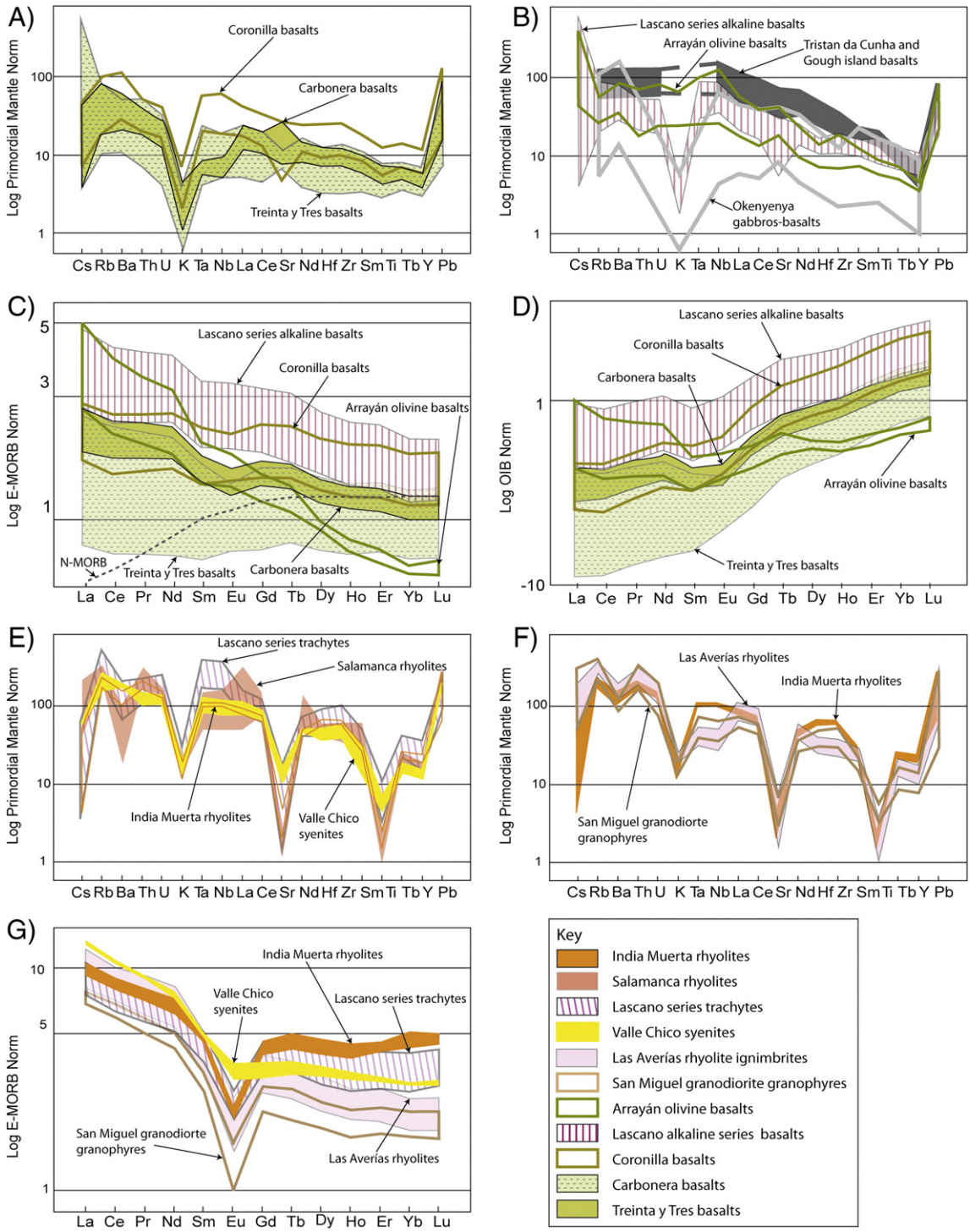

Fig. 7. Spider diagrams of whole rock trace element compositions plotted normalized to primordial mantle (McDonough et al., 1992), E-MORB and OIB (Sun and McDonough, 1989). The fields represent the variability of all the studied samples for each group. Valle Chico syenites and Salamanca and Las Averías rhyolites include samples from Kirstein et al. (2000). Tristán da Cunha samples from le Roex et al. (1990), Gough island samples from le Roex (1985) and Okenyenya gabbros–basalts samples from le Roex et al. (1996).

overlap at ~128 Ma and suggest they were both emplaced in a short time. Furthermore, rhyolite dikes similar in composition to the Salamanca rhyolite lavas intrude the syenites.

5.3. Alkaline ring complexes

Each complex is bounded by a steep magnetic and gravity gradient that is interpreted as vertical ring-fault. This fault bounds most of the highly magnetic and denser rocks inside the complexes (Fig. 2C).

5.3.1. Valle Chico

The concentric ring pattern of the magnetic anomaly at Valle Chico (Fig. 2B) could represent concentric intrusions of the highly magnetic syenites (Table 1). This is supported by the current maps of the complex that shows a central zone of coarse-grained quartz syenite rimmed on the northeast by fine- to medium-grained quartz syenite and on the southeast by syenite, quartz syenite and porphyritic trachyte (Muzio, 2000; Lustrino et al., 2005). Furthermore, the geophysical modeling by Reitmayr (2001) and Ellis and Turner (2006), argue that the source of

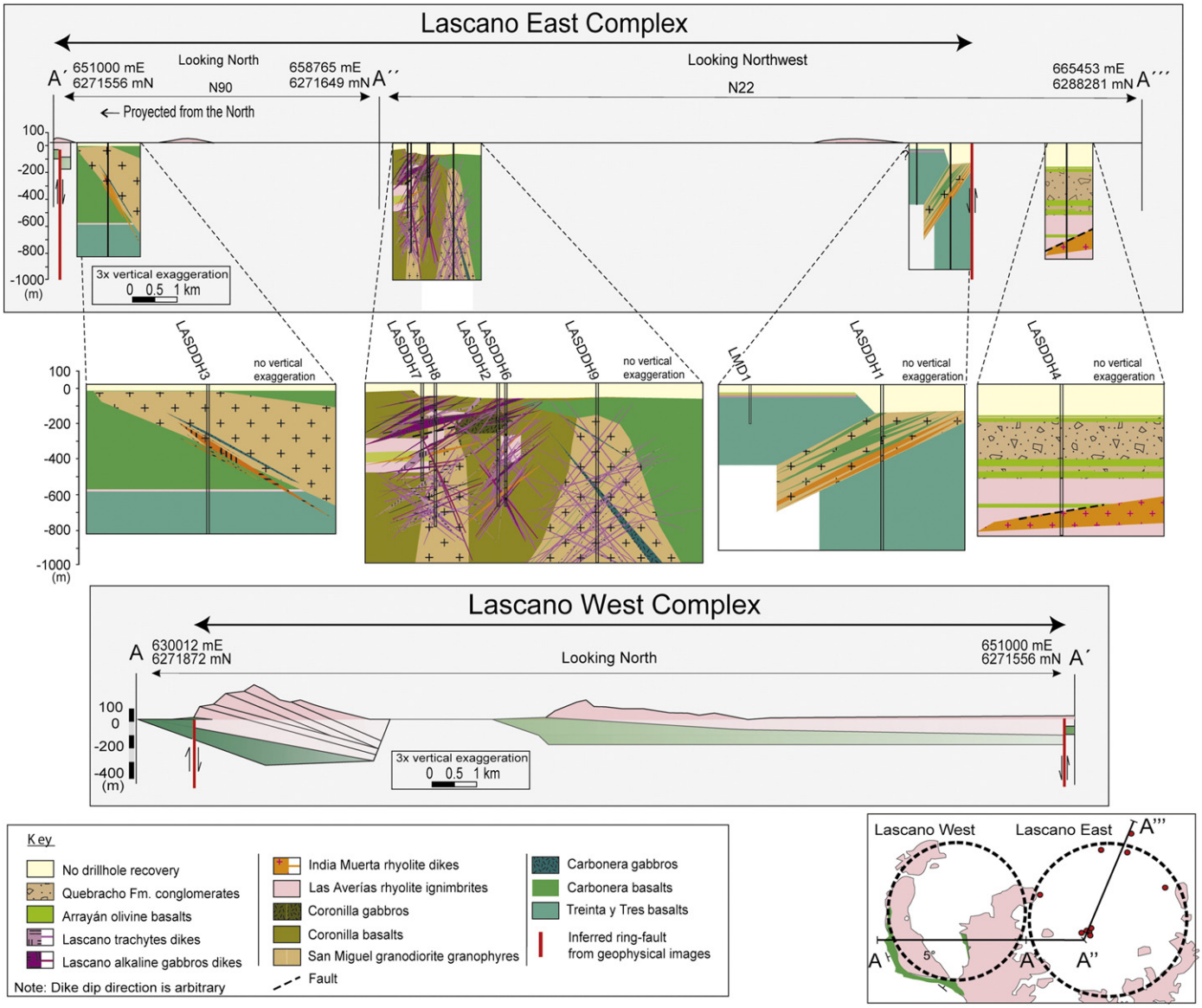

Fig. 8. Cross sections over Lascano East and West showing interpreted geology at 3× vertical exaggeration. Inserts are shown with no vertical exaggeration. Dip directions of geologic features are arbitrary since the core was not oriented.

the aeromagnetic anomalies in the Laguna Merín basin is limited to shallow crustal layers at <1 km depth. The syenites intrude the Salamanca rhyolites and are in turn cut both by rhyolitic dikes of Salamanca composition and trachyte dikes of the Lascano alkaline series. Valle Chico is the only location in the Laguna Merín basin where the Salamanca rhyolites are exposed, which suggests this ring complex may be the eruptive source of the Salamanca rhyolites.

5.3.2. Lascano East and West

The surface of Lascano West and East complexes is dominated by Las Averías rhyolite ignimbrites overlying Treinta y Tres and Carbonera basalts. At Lascano West both the ignimbrites and basalts crop out along and inside the inferred ring-fault but ignimbrites are not offset by the fault. The ignimbrites dip 2° to 5° towards the center of the ring-complex, and we interpret that they were erupted synchronously with caldera collapse along the ring-faults

In both Lascano West and East the gentle gradient of the aeromagnetic anomaly inwards from the ring-structure boundary reflects the dip of the highly magnetic Treinta y Tres and Carbonera basalts underneath the rhyolites (Fig. 4). In these complexes, the steep magnetic gradient along the ring-structure is marked by the change from positive magnetic anomaly inside against the negative magnetic anomaly outside. Therefore, the position of the steep gradient is inferred to be the ring-faulted outer contact of the magnetic basalts. This interpretation is further supported at Lascano East by drill-holes, located immediately inside the inferred ring fault, that intercepted large volumes of Treinta y Tres and Carbonera basalts and minor Las Averías rhyolites (LASDDH1, 3, LMD1). Most of the intercepted highly magnetic basalts are lava flows. Nonetheless, since the magnetic anomalies in the ring structure are broad zones and there are only three drillholes into the ring structure, the possibility of highly magnetic ring dikes that were missed by drilling is highly probable.

The large volumes of basalts and rhyolites at the rim of Lascano East ring are intruded by San Miguel granodiorite granophyres, sill-like bodies of Carbonera gabbros, and India Muerta rhyolite dikes and sills (LASDDH1, 3, 5). However, the center of the complex is composed of thin sections of Las Averías rhyolites and Treinta y Tres basalts and thick sections of Coronilla basalts. These units are not only intruded by

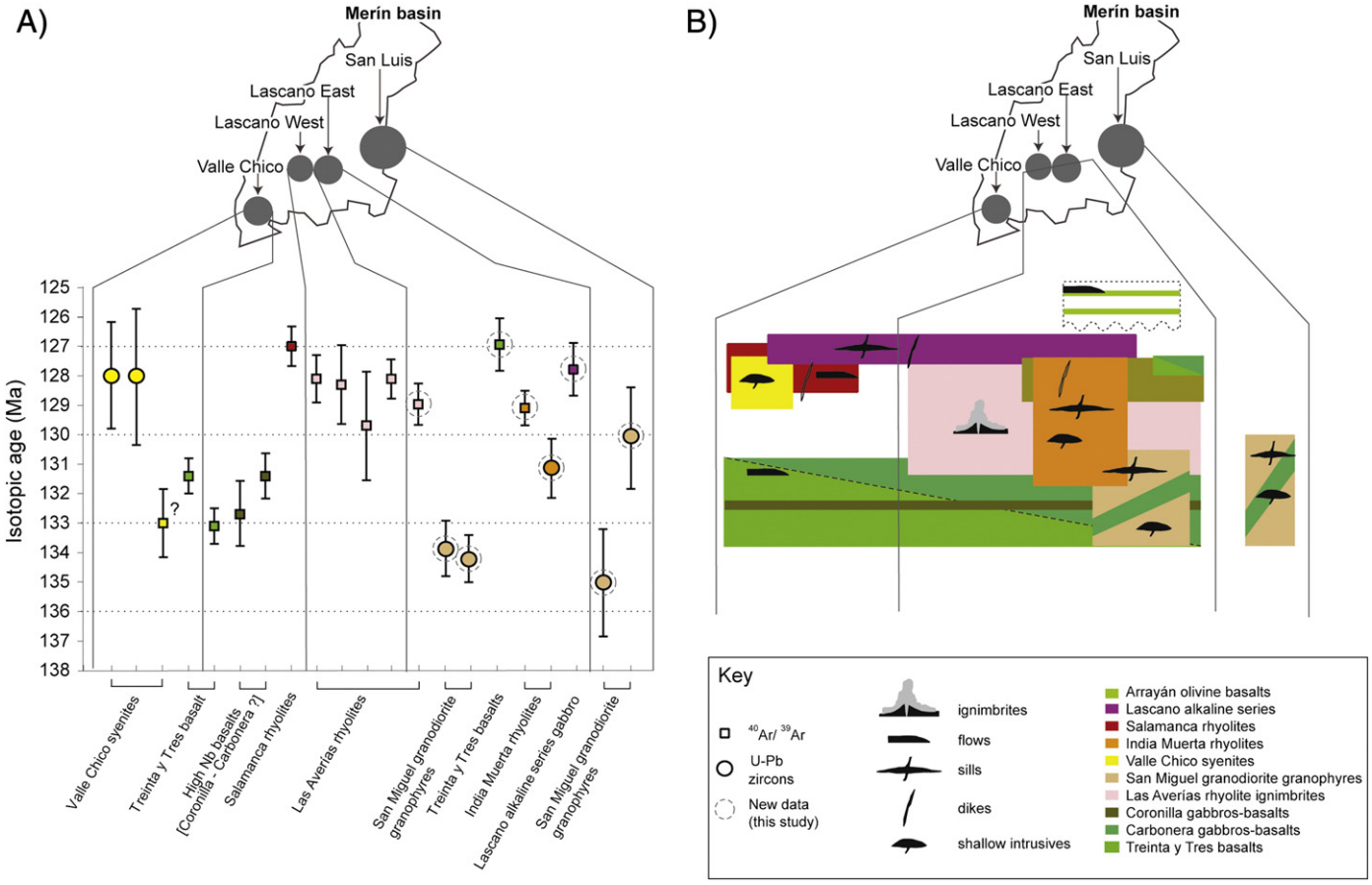

Fig. 9. A) $^{40}Ar/^{39}Ar$ and U–Pb isotopic ages of igneous rocks from the Laguna Merín basin ordered according to their geographic distribution. Error bars are two standard deviation. Data from this study and from Kirstein et al. (2001b); Stewart et al. (1996); Muzio et al. (1999) and Lustrino et al. (2005) (see Table 3). B) Synthesis of the magmatic evolution of igneous rocks in the Laguna Merín basin according to their geographic distribution, showing emplacement styles and relative age of units based on cross-cutting relations calibrated according to the isotopic ages.

San Miguel granodiorite granophyres (LASDDH8, 9) and Coronilla gabbros (LASDDH2, 6, 7), but are also heavily intruded by the Lascano alkaline series dikes and sills. Thus, the alkaline magamtism was focused in the center of the complex.

The eruption of hundreds of meters of Coronilla basalts exclusively at the center of the Lascano East complex suggests that this area was a topographic low resulting from subsidence due to the caldera collapse. These transitional basalts may represent post-collapse mafic intracaldera magmatism.

The geology outside of the Lascano East complex is contrastingly different from the geology inside. The Las Averías rhyolites and Carbonera basalts, encountered at the only drillhole outside of the Lascano East complex (LASDDH4), are located in a deeper position relative to the same lithologies inside the ring complex and are overlain by more than 400 m of Quebracho conglomerates intercalated with the Arrayán olivine basalts. These observations suggest that this boundary of the Lascano East complex was a fault that down-dropped the outside relative to the inside after the extrusion of the Las Averías ignimbrites. This is one of a pair of graben-bounding normal faults striking 250° to 260° along the north side of Lascano East that are inferred on the basis of abrupt discontinuities in aeromagnetic and gravity data (Fig. 2B). This graben is filled with the Quebracho conglomerates and Arrayán olivine basalts. The basalt and rhyolite clasts of the Quebracho Formation have compositions matching the sub-alkaline and mildly alkaline rocks, which are the most abundant rocks along the rim of the complex. Because no alkaline clasts were identified in the conglomerates, it is possible that the alkaline magmas of the Lascano series did not erupt or at least were not exposed along the scarp at the rim of the complex.

5.3.3. San Luis

The San Luis complex produces the biggest magnetic and gravity anomaly, but most of its geology is concealed, and no drill-hole data are available. The only outcrops lie immediately south of the ring-fault at its southern periphery. Small volumes of Carbonera basalts and subalkaline rhyolites are intruded by San Miguel granodiorite granophyres which are in turn cross cut by Carbonera gabbros sills.

5.4. Gravity anomalies and the mafic roots of the ring complexes

Reitmayr (2001) and Ellis and Turner (2006) calculated that the observed gravity anomaly of the Laguna Merín basin could be explained by density contrasts of at least 0.4 g/cm^3. They estimated that the dense rocks were located deeper than 1 km and inferred that they possibly extended to the upper mantle. Above, we reported density contrasts that range from 0.26 to 0.58 g/cm^3 between gabbro and less dense volcanic rocks. We propose that the gravity anomalies result from shallowly emplaced and dense Carbonera, Coronilla and Lascano gabbro dikes, sills and plugs, and additional underlying and more voluminous intrusions extending to more than 5 km depth.

An estimate of the thickness of the dense gabbroic rocks, can be calculated using the Bouguer anomaly formula ($\Delta g = 2\pi \cdot G \cdot \Delta\rho \cdot \Delta h$), where Δg is the gravity anomaly, $\Delta\rho$ is the density contrast, G is gravitational constant, and Δh is the thickness of the dense rock. To produce the observed ~80 mGal positive gravity anomaly, the calculation requires a 5 km thick body of dense rock with a ~0.4 g/cm^3 density contrast. The thickness may be greater if we visualize that the upper part of the complex is not one single intrusion, but a high density net of

gabbro dikes and sills with intervening wall-rock screens. Similar interpretations have been proposed by Bauer et al. (2003) for the ring complexes of Damaraland in Namibia.

5.5. Petrogenesis

The magmatic diversity observed in the Laguna Merín basin rocks cannot be explained simply by melting of a single source or by crystallization of a single magma. We propose that the magmatism evolved from dominantly sub-alkaline, to transitional to alkaline and hypothesize an evolution from large degrees of partial melt of a shallower N-MORB-like mantle source to lower degrees of partial melt of a deeper OIB-like source, coupled with crustal assimilation. A similar interplay between N-MORB and OIB was proposed for the formation of alkaline basalts in the Brazilian offshore rifts by Mohriak et al. (2002) and different degrees of partial melting of progressively deeper mantle sources, has been proposed for Messum and some other complexes of the Damaraland province by le Roex et al. (1996). An alternative hypothesis argues for metasomatized lithospheric mantle melts as a more likely source than a MORB-like source (Kirstein et al., 2000), however, the observed magmatic trace element enrichments are consistent with contributions of crustal assimilants and deep and enriched mantle source materials.

To test the petrogenesis of the Laguna Merín igneous rocks, linear magma mixing and fractionation/melting paths were calculated using standard approaches (Rollinson, 1993). Fractional and equilibrium crystallization paths were calculated for basalt with crystallizing proportions of 50 wt.% plagioclase, 30 wt.% clinopyroxene, 10 wt.% orthopyroxene and 10 wt.% olivine. Batch melting of lherzolite mantle was calculated using starting proportions of 50% olivine, 23% orthopyroxene and 23% clinopyroxene and 4 wt.% of an aluminum phase such as plagioclase or spinel or garnet. Mineral–melt partition coefficients and mantle source compositions were taken from Rollinson (1993), Salters and Stracke (2004) and Gurencko and Chaudisson (1994). The results of the modeling are presented here using a Nb/Zr versus La/Sm plot (Fig. 10). However, the results are similar for Ta, Hf, P, Ti, Sc, Y, Th and other rare earth element ratios such as La/Yb and Dy/Yb.

The three groups of units, sub-alkaline, transitional and alkaline, correspond to three different magmatic lineages that respond to an interplay between shallow and deep mantle melts and assimilation of different crustal rocks. These lineages can be illustrated by mixing lines between N-MORB and OIB mantle melts compositions with two Laguna Merín basin wall-rocks of Neoproterozoic age that are possible assimilants, the Santa Teresa granodiorite (STGD) and a granitic gneiss (PGN) (Fig. 10B). The N-MORB starting composition was chosen over an E-MORB composition, since the latter is too enriched to account for some of the sub-alkaline mafic rocks that present lower Nb/Zr and La/Sm compositions than an E-MORB (Fig. 10B). Therefore, the starting composition could lie between and N-MORB and an E-MORB (near primitive mantle), and could be a slightly enriched source relative to N-MORB, or could be a N-MORB derived melt that experienced some crystal fractionation (Fig. 10A).

Mixing between a shallowly derived mantle melt of N-MORB composition and the two sampled wall-rocks (i.e. crustal assimilation), associated with crystal fractionation can explain the compositional variability of the sub-alkaline and transitional rocks. Several intermediate mixing lines could be fitted with different proportions of assimilants (e.g. 10% PGN + 90% STGD, 20% PGN + 80% STGD, etc.). An assimilant composed of 80% PGN and 20% STGD is needed to explain the composition of the Treinta y Tres basalts, while an assimilant of 70% STGD and 30% PGN is needed for the Carbonera basalts (Fig. 10B). Both sub-alkaline types of basalts require at least 20% of wall-rock contamination. The sub-alkaline felsic rocks including the Las Averías rhyolites and the San Miguel granodiorites have similar origin of mixed N-MORB and PGN-STGD crust with an additional component of crystal fractionation to produce higher La/Sm values (Fig. 10B,C).

The transitional Coronilla basalts plot close to the Carbonera basalts, but displaced towards an OIB composition, which could suggest an interplay between a N-MORB and a OIB source (Fig. 10B). The transitional India Muerta and Salamanca rhyolites and the Valle Chico syenites form a trend from the Carbonera and Coronilla gabbros–basalts towards an assimilant composition intermediate between STGD and PGN (Fig. 10C). Kirstein et al. (2001a) argues for an inhibition of the fractionation of trace minerals like zircon due to the high halogen concentration in the magmas, to explain the high Nb, Zr, and Th composition of some of the felsic transitional rocks. As shown in Fig. 5, Nb and Zr concentrations increase collinearly within the fractionation trend of each unit. The same can be observed for Hf, Ta, Th and Y. This argues that both zircon and minerals that incorporate Nb (biotite, titanite, rutile) did not crystallize and are suppressed during the evolution of all the units, so that elements like Zr and Nb behave incompatibly and increase as the magmas evolve. Therefore, we think that the inhibition of the crystallization of these minerals had played a role in increasing the concentration of Zr, Hf, Th, Nb, Ta and Y in all the units, and not only in the transitional felsic rocks as previously argued.

Mixing between a deeper mantle source (40% OIB) and a shallower mantle source (60% N-MORB), or fractionated products of these, can produce a starting composition for the Lascano alkaline series. These compositions could represent physical mixtures between the two different magma sources, or lesser degree partial melting of a mantle source of intermediate depth between shallow N-MORB and deep OIB mantle source. The Arrayán olivine basalts have OIB character and are sourced more deeply than the Lascano alkaline series at lesser degrees of partial melting of an OIB mantle source.

Both the Arrayán basalts and the Lascano alkaline series compositions require the assimilation of a third type of crust (not specifically identified here) with both higher Nb/Zr and La/Sm ratios compared to STGN and PGN (Fig. 10B). As pointed out before, the suppression of zircon and titanite crystallization played a significant role in increasing the concentration of elements like Nb and Zr that remain incompatible even at high degrees of fractionation. In this way, the composition of the unknown assimilant could plot at lower Nb/Zr ratio in Fig. 10B. An alternative hypothesis to produce the high Nb/Zr and Nb/Th ratios of the alkaline rocks is melting of a previously metasomatized subcontinental lithospheric mantle as demonstrated by Pilet et al. (2008) for alkaline basalts elsewhere.

In general, melting progressively greater depths produced a continuum of melt compositions from Treinta y Tres, to Carbonera, to Coronilla, to Lascano, to Arrayán basalts. We note that this magmatic progression is in part a temporal progression, but that the field and geochronology data suggest that there is no simple temporal progression and that different compositions overlap in time. Fig. 11 illustrates that the Dy/Yb ratio increases from the sub-alkaline, to transitional, to alkaline gabbros – basalts, and reaches a maximum with the youngest Arrayán olivine basalts. High Dy/Yb indicates a garnet-bearing mantle source where garnet preferentially retains Y and heavy rare earths such as Yb, evidencing the deepening of the melts sources. The similarity of trace element contents of the Arrayán olivine basalts and the present day volcanic rocks from Gough Island and Tristan da Cunha in the southern Atlantic also supports the hypothesis that a deep OIB-like source was involved in the magma production in the late stages of the Laguna Merín basin magmatism (Figs. 7B). The deepening of the mantle source is also accompanied by progressively lower degrees of partial melting in order to explain the progressive enrichment of incompatible elements from sub-alkaline to alkaline rocks (Fig. 7).

The Nd and Sr isotope data provide further evidence that variable degrees of crustal assimilation contribute to all basic and silicic magmas in the Laguna Merín basin (Fig. 12). Even the most primitive and least contaminated samples, the Arrayán olivine basalt and the Lascano alkaline series gabbro, yield relatively evolved isotopic compositions of $^{144}Nd/^{143}Nd$ ~0.5126 and $^{87}Sr/^{86}Sr$ ~0.705 that require a small crustal component.

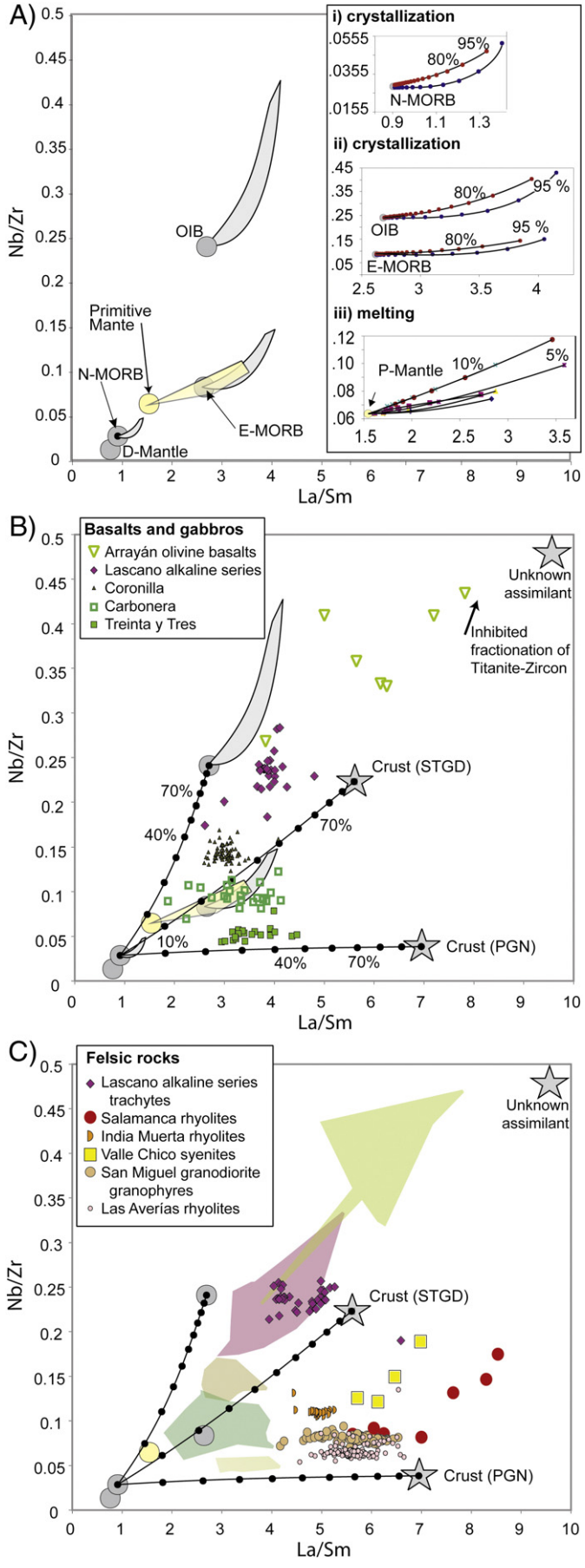

The three magmatic linages identified with the trace element modeling follow distinct paths in the $^{87}Sr/^{86}Sr$ versus $^{144}Nd/^{143}Nd$ space (Fig. 12). The sub-alkaline rocks show a trend towards lower $^{143}Nd/^{144}Nd$ and higher $^{87}Sr/^{86}Sr$ ($^{144}Nd/^{143}Nd$ ~0.5119, $^{87}Sr/^{86}Sr$ ~0.735) coincident with the isotopic compositions of the PGN (Basei et al., 2010). The transitional rocks follow a similar trend, however, they evolve to even lower $^{143}Nd/^{144}Nd$ and higher $^{87}Sr/^{86}Sr$ ($^{144}Nd/^{143}Nd$ ~0.5115, $^{87}Sr/^{86}Sr$ ~0.745), evidencing a different crustal assimilant. Kirstein et al. (2000) and Lustrino et al. (2005) previously interpreted these two trends as the result of an upper crustal assimilant for the sub-alkaline trend and a lower crust assimilant for the transitional trend. In contrast, our model, the assimilant for the sub-alkaline trend is the PGN, which is an exposed upper crustal lithology. However, the isotopic composition of the assimilant for the transitional magmatic trend remains unknown. The trace element modeling suggests the STGD is a likely assimilant, however, no isotopic data is available for STGD.

Only two samples from the Lascano alkaline series were analyzed, a gabbro and a trachyte, and they appear to form a different and third trend, not previously recognized, at higher $^{143}Nd/^{144}Nd$ (~0.5125) but with the trachyte also having a very high $^{87}Sr/^{86}Sr$, of ~0.738. This isotopic trend evidences a third and unknown crustal assimilant, that is consistent with the trace element modeling. At present, there is isotopic data only for the PGN but not other crustal basement lithologies.

5.6. Comparison with the Namibian complexes

Based on plate tectonic reconstructions for the South American and African plates at ~133 Ma, the Damaraland and Lüderitz alkaline provinces in Namibia were very close in space to the Laguna Merín basin during the early Cretaceous (Franke et al., 2007; Fig. 13). These complexes present similar size and structure, stratigraphy, and geometry of intrusions to the Laguna Merín complexes, and were emplaced between 133 and 124 Ma (Pirajno, 1994). They lie in the Paraná–Etendeka igneous province and are thought to be related to opening of the South Atlantic and the Tristan da Cunha hot spot magmatism.

The closest similarity between the Uruguayan and Namibian complexes is found in their geochemical compositions. For example, the Nb/Zr ratios of the sub-alkaline lithologies of the Okenyenya complex (formerly Okonjenje, SACS, 1980) range from 0.08 to 0.14 and overlap with the Nb/Zr ratios (0.05 to 0.10) reported in this study from the Laguna Merín basin. In contrast, the alkaline gabbros of the Okenyenya complex have a higher Nb/Zr ratio of 0.22, which is similar to the Lascano alkaline series from Laguna Merín (0.23), and very distinct from the low Nb/Zr ratio of the sub-alkaline rocks (Fig. 6). Similarly, the Nd and Sr isotopic compositions and trends of the Laguna Merín basin rocks overlap with the composition and trends of the Damaraland complexes (Fig. 12). The similarity of these chemical signatures, which primarily reflect the magma sources, together with the geochronological and paleotectonic reconstruction, indicates that the magmatism in Laguna Merín, Damaraland and Lüderitz was broadly contemporaneous

Fig. 10. Nb/Zr versus La/Sm ratio diagrams showing A) Melting and fractionation experiments showing that a unique magmatic source cannot explain the magmatic diversity found in the Laguna Merín basin. The dark grey field shows the envelope of all the fractional and batch melting experiments of a plagioclase, spinel and garnet lherzolites of primitive mantle composition. The light grey fields show all the fractional and equilibrium crystallization experiments of an average basalt from a N-MORB, E-MORB and OIB composition. The inset shows the individual melting and fractionation experiments at 5% increments. B) Whole rock composition of fresh mafic rocks samples from the Laguna Merín basin plot on top of or between mixing lines between N-MORB, OIB and possible crustal assimilants: STGD (Neoproterozoic Santa Teresa granodiorite) and PGN (Proterozoic gneiss from Cuchilla Dionisio terrane). Mixing lines are shown at 10% increments. C) Mafic rock compositions shown in B are now shown as fields, and felsic rocks compositions are plotted individually. The sub-alkaline and transitional rocks plot between N-MORB, PGN and STGD whereas the alkaline rocks plot between N-MORB, OIB and an unknown assimilant of higher Nb/Zr and La/Sm concentrations.

and probably linked to similar melt sources, evolutionary paths, and emplacement mechanisms.

In contrast to the well-exposed and partially eroded Nambian alkaline complexes, Uruguayan complexes are, except Valle Chico, poorly exposed and partly buried by young sedimentary deposits and largely expose the near surface volcanic sequence and not the subvolcanic intrusions. This is consistent with the southern end of the African plate experiencing uplift after the Gondwana break up whereas the South American plate remained more stable and low-lying as described by Moore et al. (2009). Therefore, speculations about the geology of the deeper and concealed parts of the complexes in the Laguna Merín basin can be guided by comparison with the better-exposed complexes of Damaraland.

First, the Damaraland complexes show roughly circular and steep-sided positive gravity and magnetic anomalies, of the same intensity to the ones in Laguna Merín, (e.g. Eberele et al., 2002; Bauer et al., 2003). The SIMBA seismic reflection transect over the Messum complex (Bauer et al., 2003) shows a heavily intruded root zone of cylindrical shape that extends to the Moho at ~40 km. The authors interpret this geophysical response as a network of mafic dikes, sills and small intrusions occupying 30% of the crustal column, and which increases in volume from 20 km to the Moho. The work of Bauer et al. (2003) supports the hypothesis that the gravity anomalies in the Laguna Merín basin are caused by a network of gabbroic dikes and sills and possible deeper intrusions inside each complex, and that these extend deeply into the crust.

Second, the complexes of the Damaraland present diverse lithologies that range from oversaturated complexes with granites and syenites, mixed oversaturated–undersaturated with carbonatites and undersaturated with carbonatites (Kinnaird and Bowden, 1991). With this in mind, the two concealed complexes in Laguna Merín, Lascano West and San Miguel, could be composed of different lithologies compared to the ones identified in Valle Chico and Lascano East.

Finally, the Messum ring complex exposes an inwardly gently dipping series of gabbro–rhyolite sill-like bodies and a younger central nepheline syenite, and this complex is the apparent source of the local sub-alkaline basalts, rhyolites, and alkaline rhyolites. Therefore, Messum is potentially a good model for the ring complex at 0.5–1 km depth below Lascano East and West, and was used to model Lascano-East (Fig. 14).

6. Conclusions

The magmatic evolutionary model in temporal panels shown in Fig. 14, illustrates the genesis of the Lascano East complex. Based on the observations presented above, the genesis of Lascano West is likely similar.

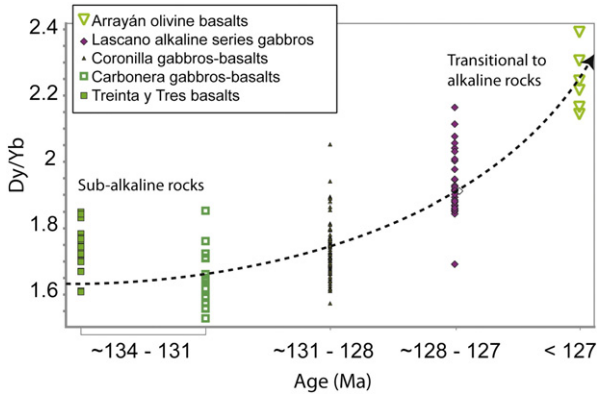

Fig. 11. Dy/Yb ratio for different mafic lithogeochemical units grouped according to their alkalinity. This trend reflects a progressive deepening of the mantle source and/or smaller degrees of partial melting from the sub-alkaline gabbro–basalts to the younger alkaline gabbro–basalts.

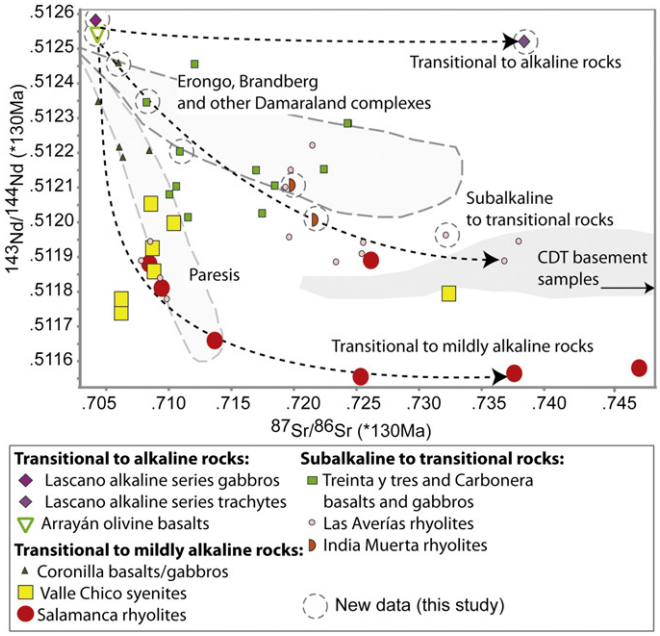

Fig. 12. Isotope ratio plot showing that all the rocks from the Laguna Merín basin show high $^{87}Sr/^{86}Sr$ and low $^{144}Nd/^{143}Nd$, ratios evidencing abundant crustal assimilation in their petrogenesis. The compositions are comparable to similar complexes from the Damaraland Alkaline Province in Namibia shown as fields (from Lustrino et al., 2005). The sub-alkaline, mildly alkaline and alkaline rocks show different evolutionary trends in the isotopic space, with the sub-alkaline rocks overlapping with the available isotopic compositions of the Proterozoic wall-rock (data from Basei et al., 2011).

Rifting related to the opening of the South Atlantic produced asthenospheric ascent and decompression, which triggered partial melting to produce basaltic magmas at different depths. The early stages

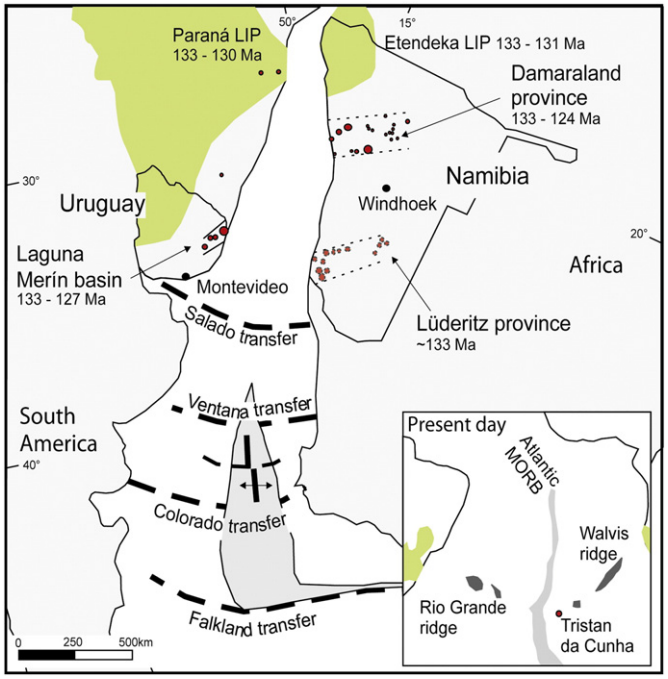

Fig. 13. Paleogeographical reconstruction of southern Gondwana at ~133 Ma taken from Jokat et al. (2003), Macdonald et al. (2003) and Franke et al. (2007) (Azimuthal equal area projection centered at 40° S, 0° E) showing Paraná–Etendeka large igneous province, the Laguna Merín basin and its intrusive complexes in Uruguay, Damaraland intrusive complexes (location from Google Earth, Milner and le Roex, 1996; Pirajno, 2009) and Lüderitz intrusives complexes (locations from Pirajno, 1994) in Namibia. Ticks show present day latitude and longitude in WGS84. Insert shows present day geography and location of Tristan da Cunha island.

were dominated by large degrees of partial melt of a shallow-source and were broadly tholeiitic. These melts assimilated gneisses and granitoids of the Proterozoic Cuchilla Dionisio terrane together with crystal fractionation generated the sub-alkaline magmatic rocks. They erupted between 134 and 131 Ma as the Treinta y Tres and Carbonera sub-alkaline basalts and possibly minor amounts of the transitional Coronilla basalts. After the first eruptions, the San Miguel granodiorite granophyres, products of extensive crustal melting and mixing with basalt, and the Carbonera gabbros intruded shallowly and principally as sill-like bodies.

At least two shallow silicic magma chambers developed in the Lascano East and West ring complexes, and erupted to form the Las Averías rhyolite ignimbrites between 131.5 and 128 Ma. The voluminous Las Averías rhyolite ignimbrites rapidly erupted, emptied the magmatic chambers, and produced caldera collapse along ring-faults. This collapse caused sagging and the inward tilting of the Treinta y Tres and Carbonera basalts and Las Averías ignimbritc rhyolites inside the Lascano East and West calderas. These ignimbrites were deformed to dip gently inward during the subsidence of the caldera floor. Less voluminous batches of the sub-alkaline basalts of Treinta y Tres and Carbonera were extruded at this time intercalated with individual Las Averías ignimbrite eruptions.

At the same time, the Coronilla basalts lavas erupted inside the Lascano East caldera, as part of the intracaldera magmatism, and were accompanied by the emplacement of chemically similar gabbro dikes and sills.

In the final stages, between 128 and 127 Ma, the India Muerta rhyolite dikes were emplaced and were followed by the Lascano alkaline series intrusions, as dikes, sills and plugs of alkaline gabbro to trachyte. Minor amounts of late sub-alkaline basalts might have also been extruded at this stage. In contrast to the sub-alkaline rocks, the transitional and alkaline igneous rocks were produced by progressively deepening of the mantle melting source and lessening of the degree of partial melting and assimilation of the Neoproterozic Santa Teresa granodiorite and other un-identified wall-rock lithologies together with crystal fractionation.

The density contrast of ~0.4 g/cm^3 between the gabbro dikes and sills with the rest of the rocks is coincident with the estimated contrast to satisfy previous geophysical models and suggests that these are responsible for the gravity anomalies. On the basis of geophysical data,

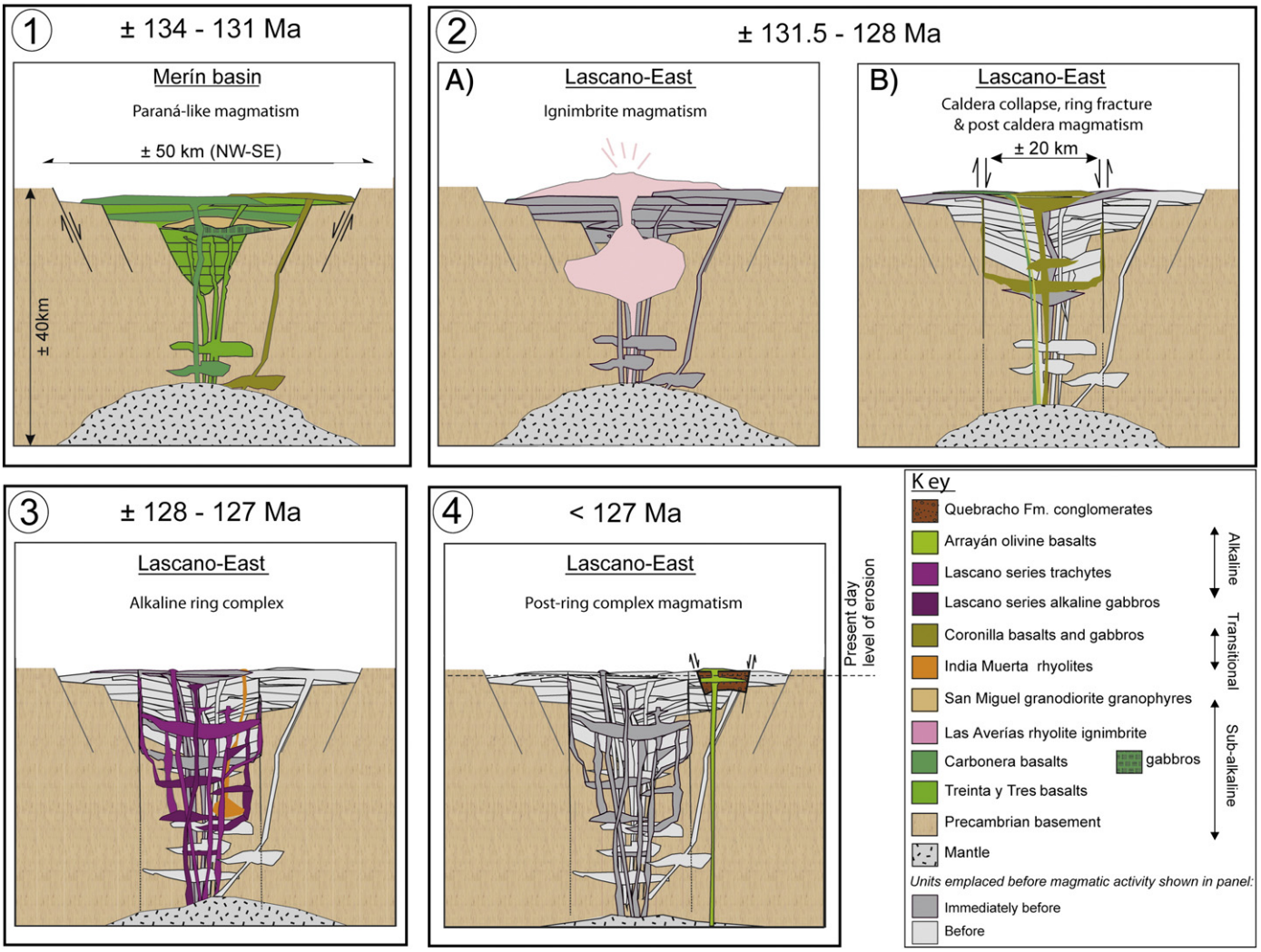

Fig. 14. Simplified evolution of the magmatism in the Laguna Merín basin and Lascano East represented in temporal panels. 1) Initial stages of magmatism in the Laguna Merín basin dominated by the extrusion of large volumes of sub-alkaline basalts and associated gabbros and granodiorite intrusions. Only minor volumes of mildly-alkaline basalts where extruded at this time. 2A) Formation of sub-alkaline felsic magma chambers in Lascano East and West and extrusion of large volumes of rhyolite ignimbrites that produced the 2B) collapse of the volcanic calderas and the formation of ring-faults followed by intra-caldera extrusion of sub-alkaline to mildly-alkaline basalts and intrusion of dikes of similar compositions. 3) Intrusion of the Lascano alkaline series reutilizing the sub-alkaline feeder zones and the ring-faults. 4) Waning stages of the magmatic system and extrusion of small volumes of alkaline olivine basalts outside of the complex.

a dense net of mafic intrusions was likely deeply emplaced during this stage and was the source of the shallow dike and sills.

Lastly, after ~127 Ma, the Arrayán olivine basalts erupted peripheral to Lascano East, and flooded the low topography areas formed by down-dropped blocks along east–west striking normal faults outside of the ring structure.

Acknowledgments

This research was fully funded by Orosur Mining Incorporated (OMI) and Oregon Laurels scholarship from Oregon State University. Many thanks to Nestor Vaz, Devin Den Boer, Pedro Oyhantçabal, Carmen Álvez and Nora Lorenzo for the logistical help of the OMI organization, and helpful discussions. Thanks are due to Dr. Robert Harris for the discussion of geophysical data, Martín Rodríguez for great help in sampling drillhole core and to Morgan Salisbury for reviewing the English of early versions of this paper. Ruben Padilla and Anglo Gold Ashanti provided the U–Pb zircon age determinations made at the University of Arizona. Thoughtful reviews by Linda Kirstein and Claudio Gaucher enriched the article and are greatly appreciated.

Appendix A. Supplementary data

Supplementary data to this article can be found online at http://dx.doi.org/10.1016/j.gr.2014.07.007.

References

Almeida, F.F.M., 1983. Relações tectônicas das rochas alcalinas mesozóicas da região meridional da plataforma sul-americana. Revista Brasileira de Geociencias 13, 139–158.

Basei, M.A.S., Siga Jr., O., Masquelin, H., Harara, O.M., Reis Neto, J.M., Preciozzi, F., 2000. The Dom Feliciano Belt (Brazil–Uruguay) and its Foreland, the Rio de la Plata Craton: framework, tectonic evolution and correlations with similar provinces of southwestern Africa. In: Cordani, U., Milani, E., Thomaz Filho, A., Campos, D. (Eds.), Tectonic Evolution of South America, 31st International Geological Congress, Rio de Janeiro, Brazil. FINEP, Rio de Janeiro, pp. 311–334.

Basei, M.A.S., Peel, E., Sánchez Bettucci, L., Preciozzi, F., Nutman, A.P., 2010. The basement of the Punta del Este Terrane (Uruguay): an African Mesoproterozoic fragment at the eastern border of the South American Río de La Plata craton. International Journal of Earth Sciences 100 (2–3), 289–304. http://dx.doi.org/10.1007/s00531-010-0623-1.

Basei, M.A.S., Peel, E., Sánchez Bettucci, L., Preciozzi, L., Nutman, A.P., 2011. The basement of the Punta Del Este terrane (Uruguay): an African Mesoproterozoic fragment at the eastern border of the southamerican Río de La Plata craton. International Journal of Earth Sciences 100 (2–3), 289–304.

Basei, M.A.S., Sánchez Bettucci, L., Peel, E., Muzio, R., 2013. Geocronología U–Pb LA-ICP-MS en circones del Complejo Granítico Santa Teresa, Terreno Punta del Este. VII Congreso Uruguayo de Geología and I Simposio Minería y Desarrollo del Cono Sur, Programa. Centro de Pesquisas Geocronológicas – Universidade de São Paulo, Montevideo, pp. 30–31.

Bauer, K., Trumbull, R.B., Vietor, T., 2003. Geophysical images and crustal model of intrusive structures beneath the Messum ring complex, Namibia. Earth and Planetary Science Letters 216, 65–80.

Bellieni, G., Comin-Chiaramonti, P., Marques, L.S., Melfi, A.J., Nardy, J.R., Papatrechas, C., Piccirillo, E.M., Roisenberg, A., Stolfa, D., 1986. Petrogenetic aspects of acid and basaltic lavas from the Parana Plateau (Brazil): geological, mineralogical and petrochemical relationships. Journal of Petrology 27, 915–944.

Biondi, J.C., 2003. Processos metalogenéticos e os depósitos minerais brasileiros. São Paulo, Oficina de textos, (528 pp.).

Bossi, J., Ferrando, L.A., 2001. Carta Geológica Del Uruguay a Escala 1/500.000; Versión Digital 2.0 En CD-ROM. Facultad de Agronomía.

Bossi, J., 1966. Recursos minerales del UruguayColección Nuestra Tierra. Ediciones Aljanati, Montevideo 10, 68.

Bossi, J., Gaucher, C., 2004. The Cuchilla Dionisio Terrane, Uruguayan allochthonous block accreted in the Cambrian to SW Gondwana. Gondwana Research 2, 661–674.

Bossi, J., Ferrando, L., Montaña, J., Campal, N., Morales, H., Gancio, F., Schipilov, A., Piñeyro, D. and Sprechmann, P., 1998. Carta Geológica del Uruguay, a Escala 1/500.000 Versión 1.0 Digital. Geoeditores-Facultad de Agronomía, Montevideo.

Bossi, J., Pineyro, D., Cingolani, C.A., 2005. El límite sur del Terreno Piedra Alta (Uruguay). Importancia de la faja milonítica sinistral de Colonia. Actas XVI Congreso Geológico Argentino. 1, pp. 173–180.

Comin-Chiaramonti, P., Cundari, A., Degraff, J.M., Gomes, C.B., Piccirillo, E.M., 1999. Early Cretaceous–Tertiary magmatism in eastern Paraguay (western Paraná basin): geological, geophysical and geochemical relationships. Journal of Geodynamics 28, 375–391.

Comin-Chiaramonti, P., Gomes, C.B., Castorina, F., Censi, P., Antonini, P., Furtado, S., Ruberti, E., Scheibe, L.F., 2002. Geochemistry and geodynamic implications of the Anitapolis and Lages alkaline–carbonatite complexes, Santa Catarina State, Brazil. Revista Brasileira de Geociencias 32, 43–58.

Conti, B., 2008. Caracterización faciológica y estructural del magmatismo Mesozoico en la región de Lascano. (Undergraduate thesis) Facultad de Ciencias, UDELAR, Montevideo, (85 pp.).

Darbyshire, D.P.F., Fletcher, C.J.N., 1979. A Mesozoic alkaline province in eastern Bolivia. Geology 7, 545–548.

De Santa Ana, H., Ucha, N., 1994. Exploration, perspectives and hydrocarbon potential of the Uruguayan sedimentary basins. ANCAP, Montevideo, (90 pp.).

Deckart, K., Feraud, G., Marques, L.S., Bertrand, H., 1998. New time constraints on dyke swarms related to the Paraná–Etendeka magmatic province, and subsequent south Atlantic opening, southeastern Brazil. Journal of Volcanology and Geothermal Research 80, 67–83.

Dumitru, T.A., Ernst, W.G., Wright, J.E., Wooden, J.L., Wells, R.E., Farmer, L.P., Kent, A.J.R., Graham, S.A., 2013. Eocene extension in Idaho generated massive sediment floods into the Franciscan Trench and into the Tyee, Great Valley, and Green River Basins. Geology 41 (2), 187–190.

Eberele, D.G., Andritzky, G., Hutchins, D.G., Wackerle, R., 2002. The regional magnetic data set of Namibia: compilation, contributions to crustal studies and support to natural resource management. South African Journal of Geology 205, 361–380.

Ellis, T., Turner, R., 2006. Progress report on the evaluation of the air-FTG gravity gradiometer and aeromagnetic surveys on the Lascano project, Uruguay. Internal Orosur Mining INC, (November 15th, 2006).

Erlank, A.J., Marsh, J.S., Duncan, A.R., Miller, R. McG, Hawkesworth, C.J., Betton, P.J., Rex, D.C., 1984. Chemistry and petrogenesis of the Etendeka volcanic rocks from SWA/Namibia. In: Erlank, A.J. (Ed.), Petrogenesis of the Volcanic Rocks of the Karoo Province. Geological Society of South Africa, Special Publication. 13, pp. 195–245.

Ernesto, M., Raposo, M.I.B., Marques, L.S., Renne, P.R., Diogo, L.A., De Min, A., 1999. Paleomagnetism, geochemistry and $^{40}Ar/^{39}Ar$ dating of the north-eastern Paraná Magmatic Province. Tectonic Implications. Journal of Geodynamics 28, 321–340.

Farmer, L.P., 2012. Trace element characteristics of zircon: a means of assessing mineralization potential of intrusions in northern Nevada. (MS thesis) Oregon State University, (108 pp.).

Ferrando, L., Fernández, A.N., 1971. Esquema tectono-cronoestratigráfico del Predevoniano en el Uruguay. Anais XXV Congresso Brasileiro de Geologia, SBG, Sao Paulo, pp. 199–210.

Fletcher, C.J.N., Beddoe-Stephens, B., 1987. The petrology, chemistry and crystallization history of the Velasco alkaline province, eastern Bolivia. In: Fitton, J.G., Upton, B.G.J. (Eds.), Alkaline Igneous RocksGeological Society Special Publication. 30. Blackwell, pp. 403–413.

Franke, D., Neben, S., Ladage, S., Schreckenberger, B., Hinz, K., 2007. Margin segmentation and volcano-tectonic architecture along the volcanic margin of Argentina/Uruguay, South Atlantic. Marine Geology 244 (1), 46–67.

Gaucher, C., Frimmel, H.E., Germs, G.J.B., 2009. Tectonic events and palaeogeographic evolution of southwestern Gondwana in the Neoproterozoic and Cambrian. In: Gaucher, C., Sial, A.N., Halverson, G.P., Frimmel, H.E. (Eds.), Neoproterozoic–Cambrian Tectonics, Global Change and Evolution: a focus on southwestern GondwanaDevelopments in Precambrian Geology. 16. Elsevier, pp. 295–316.

Gehrels, G.E., Valencia, V., Pullen, A., 2006. Detrital zircon geochronology by Laser-Ablation Multicollector ICPMS at the Arizona LaserChron Center. In: Loszewski, T., Huff, W. (Eds.), Geochronology: Emerging Opportunities, Paleontology Society Short Course: Paleontology Society Papers. 11 (10 pp.).

Gehrels, G.E., Valencia, V.A., Ruiz, J., 2008. Enhanced precision, accuracy, efficiency, and spatial resolution of U–Pb ages by laser ablation-multicollector-inductively coupled plasma-mass sectrometry. Geochemistry, Geophysics, Geosystems 9 (3), 1525–2027.

GEOROC, C. http://georoc.mpch-mainz.gwdg.de/georoc/ (Visited on 20th January, 2011).

Gomes, C.B., Comin-Chiaramonti, P., 2005. An introduction to the alkaline and alkaline-carbonatitic magmatism in and around the Paraná basin. In: Comin-Chiaramonti, P., Gomes, C.B. (Eds.), Mesozoic to Cenozoic Alkaline Magmatism in the Brazilian Platform. Edusp, Sao Paulo, Brazil, pp. 21–30.

Gómez Rifas, C., Masquelin, H., 1996. Petrología y geoquímica de las rocas volcánicas cretáceas del Uruguay. XII Congreso Geológico Argentino—III Congreso de Exploración de Hidrocarburos. 3, pp. 635–652.

Gurencko, A.A., Chaudisson, M., 1994. Enriched and depleted primitive melts included in olivine from Icelandic tholeiites: origin by continuous melting of a single mantle column. Geochimica et Cosmochimica Acta 59 (14), 2905–2917.

Hartmann, L.A., Santos, J.O., Bossi, J., Campal, N., Schipilov, A., Mac Naughton, N.J., 2002. Zircon and titanite U–Pb SHRIMP geochronology of Neoproterozoic felsic magmatism on the eastern border of the Rio de la Plata Craton, Uruguay. Journal of South American Earth Sciences 15, 229–236.

Hawkesworth, C.J., Mantovani, M.S.M., Peate, D.W., 1988. Lithosphere remobilisation during Parana magmatism. In: Cox, K.G., Menzies, M.A. (Eds.), Oceanic and Continental Lithosphere: Similarities and Differences. Journal of Petrology Special Volume, pp. 205–223.

Hawkesworth, C., Kelley, S., Turner, S., le Roex, A., Storey, B., 1999. Mantle processes during Gondwana break-up and dispersal. Journal of African Earth Sciences 28, 239–261.

Irvine, T.A., Baragar, W.R.A., 1971. A guide to the chemical classification of the common volcanic rocks. Canadian Journal of Earth Sciences 8, 523–548.

Jokat, W., Boebel, T., König, M., Meyer, U., 2003. Timing and geometry of early Gondwana breakup. Journal of Geophysical Research 108, 1–19.

Kinnaird, A.J., Bowden, P., 1991. Magmatism and mineralization associated with Phanerozoic anorogenic plutonic complexes of the African Plate. In: Kampunzu, A.B., Lubala, R.T. (Eds.), Magmatism in Extensional Structural Settings: The Phanerozoic African Plate. Springer-Verlag, Berlin, pp. 410–485.

Kirstein, L.A., Peate, D.W., Hawkesworth, C.J., Turner, S.P., Harris, C., Mantovani, M.S.M., 2000. Early Cretaceous basaltic and rhyolitic magmatism in southern Uruguay associated with the opening of the south Atlantic. Journal of Petrology 41, 1413–1438.

Kirstein, L.A., Hawkesworth, C.J., Garland, F.G., 2001a. Felsic lavas or rheomorphic ignimbrites: is there a chemical distinction? Contributions to Mineralogy and Petrology 142, 309–322.
Kirstein, L.A., Kelley, S., Hawkesworth, C., Turner, S., Mantovani, M., Wijbrans, J., 2001b. Protracted felsic magmatic activity associated with the opening of the South Atlantic. Journal of the Geological Society of London 158, 583–592.
Koppers, A., Duncan, B., 2003. High-resolution $^{40}Ar/^{39}Ar$ dating of the oldest oceanic basement basalts in the western Pacific basin. Geochemistry, Geophysics, Geosystems 4 (11), 1–20.
Le Maitre, R.W., Bateman, P., Dudek, A., Keller, J., Lameyre, J., Le Bas, M.J., Sabine, P.A., Schmid, R., Sorensen, H., Streckeisen, A., Woolley, A.R., Zanettin, B., 1989. A Classification of Igneous Rocks and Glossary of Terms: Recommendations of the International Union of Geological Sciences Subcommission on the Systematics of Igneous Rocks. Blackwell Scientific, Oxford.
le Roex, A.P., 1985. Geochemistry, mineralogy and magmatic evolution of the basaltic and trachyte lavas from Gough Island, South Atlantic. Journal of Petrology 26 (1), 149–186.
le Roex, A.P., Cliff, R.A., Adair, B.J.I., 1990. Tristan da Cunha, South Atlantic: geochemistry and petrogenesis of a basanite–phonolite lava series. Journal of Petrology 31 (4), 299–812.
le Roex, A.P., Watkins, R.T., Reid, A.M., 1996. Geochemical evolution of the Okenyenya sub-volcanic ring complex, northwestern Namibia. Geological Magazine 133, 645–670.
le Roex, A.P., Chevallier, L., Verwoerd, W.J., Barends, R., 2012. Petrology and geochemistry of Marion and Prince Edward islands, Southern Ocean: magma chamber processes and source region characteristics. Journal of Volcanology and Geothermal Research 223, 11–28.
Loewen, M.W., Kent, A.J.R., 2012. Sources of elemental fractionation and uncertainty during the analysis of semi-volatile metals in silicate glasses using LA-ICP-MS. Journal of Analytical Atomic Spectrometry 27 (9), 1502–1508.
Lustrino, M., Melluso, L., Brotzu, P., Gomes, C.B., Morbidelli, L., Muzio, R., Ruberti, E., Tassinari, C., 2005. Petrogenesis of the early Cretaceous Valle Chico igneous complex (SE Uruguay): relationships with Paraná–Etendeka magmatism. Lithos 82, 407–434.
Macdondald, D., Gomez-Pereza, I., Franzese, J., Spalletti, L., Lawver, L., Gahagan, L., Dalziel, I., Thomas, C., Trewind, N., Hole, M., Paton, D., 2003. Mesozoic break-up of SW Gondwana: implications for regional hydrocarbon potential of the southern South Atlantic. Marine and Petroleum Geology 20, 287–308.
Madeisky, H.E., Stanley, C.R., 1993. Lithogeochemical exploration for metasomatic zones associated with volcanic-hosted massive sulphide deposits using pearce element ratio analysis. International Geology Review 35, 1121–1148.
Mallman, G., Chemale Jr., F., Morales, L.F.G., 2004. Evolução estrutural da porção sul do terreno Nico Pérez, Uruguay: Registro da convergência entre as placas Rio de la Plata e Kalahari no final do Neoproterozóico. Revista Brasileira de Geociências 34 (2), 201–212.
Masquelin, H., 2006. El Escudo uruguayo. In: Veroslavsky, G., Ubilla, M., Martinez, S. (Eds.), Cuencas sedimentarias de Uruguay: Paleozoico. Dirac, Montevideo, pp. 37–106.
McDonough, W.F., Sun, S.S., Ringwood, A.E., Jagoutz, E., Hofmann, A.W., 1992. Potassium, rubidium and cesium in the Earth and Moon and the evolution of the mantle of the Earth. Geochimica et Cosmochimica Acta 56, 1001–1012.
Miller, R.Mc.G., 2008. The Geology of Namibia. Volume 3: Upper Paleozoic to Cenozoic: Sections 18 and 19Published by the Ministry of Mines and Energy Geological Survey of Namibia.
Milner, S.C., le Roex, A.P., 1996. Isotope characteristics of the Okenyenya Igneous Complex, Northwestern Namibia: constraints on the composition of the Early Tristan Plume and the origin of the EM 1 Mantle Component. Earth and Planetary Science Letters 141 (1–4), 277–291.
Mincato, R.L., Enzweiler, J., Schrank, A., 2003. Novas idades $^{40}Ar/^{39}Ar$ e implicações na metalogênese dos depósitos de sulfetos magmáticos de Ni–Cu–EPG na Província Ígnea Continental do Paraná. SBGq, Congresso Brasileiro de Geoquímica, 9, Extended abstracts, pp. 67–92.
Mohriak, W.U., Rosendahl, B.R., Turner, J.P., Valente, S.C., 2002. Crustal architecture of South Atlantic volcanic magin. In: Menzies, M.A., Klemperer, S.L., Ebinger, C.J., Baker, J. (Eds.), Volcanic of Rifted Margins. GSA special paper. 362, pp. 159–202.
Moore, A., Blenkinsop, T., Cotterill, F., 2009. Southern African topography and erosion history: plumes or plate tectonics? Terra Nova 21, 310–315.
Morales, E., 2006. Caracterización faciológica de los depósitos volcánicos mesozoicos asociados a la Formacion Arequita (Ki). Uruguay. (Undergraduate thesis) UDELAR Montevideo (64 pp.).
Morales, E., Muzio, R., Veroslavsky, G., Conti, B., 2006. Geología de la Sierra de los Ajos (Cuenca Laguna Merín, Rocha, Uruguay). Revista de la Sociedad Uruguaya de Geología 13, 4–10.
Morbidelli, L., Gomes, C.B., Beccaluva, L., Brotzu, P., Conte, A.M., Ruberti, E., Traversa, G., 1995. Mineralogical, petrological and geochemical aspects of alkaline and alkaline–carbonatite associations from Brazil. Earth Science Reviews 39, 135–168.
Muzio, R., 2000. Evolucáo petrológica e geocronologia do Macico alcalino Valle Chico, Uruguay. (PhD thesis) Instituto de Geociências e Ciencias Exatas—Universidade Estadual Paulista, Rio Claro, Brazil, (171 pp.).
Muzio, R., Peel, E., Artur, A.C., 1999. New geochronological data of the Valle Chico alkaline massif (Uruguay) using U-Pb and Sm-Nd systematics. II Simposio Sudamericano de Geología Isotópica, pp. 82–85.
Muzio, R., Peel, E., Morales, E., 2009. Mesozoic magmatism in East Uruguay: petrological constraints related to the Sierra de San Miguel region. Earth Sciences Research Journal 13 (1), 16–29.
NORMS, S. http://minerva.union.edu/hollochk/c_petrology/norms.htm (Visited on 20th January, 2011).
O'Connor, J.M., Duncan, R.A., 1990. Evolution of the Walvis ridge–Rio Grande rise hot spot system. Implication for African and South American plates over plumes. Journal of Geophysical Research 95, 17475–17502.
Oyhantçabal, P.B., Siegesmund, S., Wemmer, K., Presnyakov, S., Layer, P., 2009. Geochronological constraints on the evolution of the southern Dom Feliciano Belt (Uruguay). Journal of the Geological Society of London 166, 1075–1084.
Peate, D.W., Hawkesworth, C.J., 1996. Lithospheric to asthenospheric transition in Low-Ti flood basalts from southern Paraná, Brazil. Chemical Geology 127, 1–24.
Pilet, S., Baker, M.B., Stolper, E.M., 2008. Metasomatized lithosphere and the origin of alkaline lavas. Science 320 (5878), 916–919.
Pirajno, F., 1994. Mineral resources of anorogenic alkaline complexes in Namibia: a review. Australian Journal of Earth Sciences 41, 157–168.
Pirajno, F., 2009. Hydrothermal Processes and Mineral Systems. Springer, (1250 pp.).
Preciozzi, F.L., Masquelin, H., Basei, M.A.S., 1999. The Namaqua/Greenvile Terrane of eastern Uruguay. II South American Symposium on Isotope Geology, Argentina, pp. 338–340.
Reitmayr, G., 2001. Una espectacular peculiaridad uruguaya: la anomalía gravimétrica de la Laguna Merín. 15° Congreso Latinoamericano de Geología, 3° Congreso Uruguayo de Geología, Actas Digitales, Montevideo.
Renne, P.R., Ernesto, M., Pacca, I.G., Coe, R.S., Glen, J.M., Prévot, M., Perrin, M., 1992. The age of Paraná flood volcanism, rifting of Gondwanaland and the Jurassic–Cretaceous boundary. Science 258, 975–979.
Renne, P.R., Ernesto, M., Milner, S.C., 1997. Geochronology of the Parana–Etendeka magmatic province. EOS, American Geophysical Union 78 (46), 742.
Rollinson, H.R., 1993. Using Geochemical Data: Evaluation, Presentation, Interpretation. J. Wiley & Sons, New, (352 pp.).
Rosello, E.A., de Santa Ana, H., Veroslavsky, G., 1999. El lineamiento Santa Lucía-Aiguá-Merín (Uruguay): Un rifting transtensivo Mesozoico abortado durante la apertura atlántica? Anais 5to simposio sobre o Cretáceo do Brasil and 1er simposio sobre el Cretácico de America del Sur, UNSP/SBG, Serra Negra, Brasil, pp. 443–448.
SACS, 1980. Stratigraphy of South Africa. Part 1. Lithostratigraphy of the Republic of S.A., South West Africa/Namibia and the Republics of Bophuthatswana, Transkei and Venda. Handbook of the Geological Survey of South Africa.
Salisbury, M.J., Jicha, B.R., de Silva, S.L., Singer, B.S., Jimenez, N., Ortiz, M.H., 2010. $^{40}Ar/^{39}Ar$ chronostratigraphy of Altiplano-Puna volcanic complex ignimbrites reveals the development of a major magmatic province. Geological Society of America Bulletin 123 (1), 1–20.
Salters, V.J.M., Stracke, A., 2004. Composition of the depleted mantle. Geochemistry, Geophysics, Geosystems 5 (5), 1–27.
Salvador, A., 1994. International Stratigraphic Guide, A guide to stratigraphic classification, terminology and procedure2nd edition. IUGS-GSA, Boulder, pp. 1–214.
Sánchez-Bettucci, L., Mezzano, A., 1993. Análisis sedimentológico y faciológico de la Formación Rocha (ex-Grupo Rocha). Revista Brasileira de Geociencias 23, 323–329.
Servicio Geográfico Militar, 1973. Carta gravimétrica provisoria de la República Oriental del Uruguay. Scale 1:1,000,000. Eds. SGM ROU, Montevideo, Uruguay.
Stewart, K., Turner, S., Kelley, S., Hawkesworth, C., Kirstein, L. And, Mantovani, M., 1996. 3-D, 40Ar–39Ar geochronology in the Parana' continental flood basalt province. Earth and Planetary Science Letters 143, 95–109.
Sun, S.S., McDonough, W.F., 1989. Chemical and isotopic systematics of oceanic basalt, implications for the mantle composition and processes. In: Saunders, A.D., Norry, M.J. (Eds.), Magmatism in the Ocean Basins. Geological Society Special Publication. 42, pp. 313–345.
Turner, S., Regelous, M., Kelley, S., Hawkesworth, C., Mantovani, M., 1994. Magmatism and continental break-up in the South Atlantic: high precision $^{40}Ar/^{39}Ar$ geochronology. Earth and Planetary Science Letters 121, 333–348.
Turner, S., Peate, D., Hawkesworth, C., Peate, D., Hallinan, S., Mantovani, M., 1999. Petrogenesis of an 800 metre lava sequence in Eastern Uruguay: insights into magma chamber processes beneath the Paraná flood basalt province. Journal of Geodynamics 28, 471–487.
Veroslavsky, G., Rossello, E.A., De Santa Ana, H., 2002. La anomalía gravimétrica de la Laguna Merín: origen y expectativas en la exploración mineral. Revista de la Sociedad Uruguaya de Geología 1 (2), 21–28.